Available online at www.sciencedirect.com
ScienceDirect
Geochimica et Cosmochimica Acta 71 (2007) 1–24
Geochimica
www.elsevier.com/locate/gca

A surface complexation model for sulfate and selenate on iron oxides consistent with spectroscopic and theoretical molecular evidence

Keisuke Fukushi [1], Dimitri A. Sverjensky *

Department of Earth and Planetary Sciences, Johns Hopkins University, Baltimore, MD 21218, USA

Received 23 March 2006; accepted in revised form 1 August 2006

Abstract

Sulfate and selenate adsorption on iron oxides are important reactions in natural systems under a very wide range of pH values, ionic strengths, and electrolyte compositions. Under such conditions, spectroscopic and theoretical calculations have demonstrated the potential importance of a variety of surface species. Understanding the variations in the surface speciation of these oxyanions is fundamental to prediction of their partitioning between minerals and aqueous solutions. In the present study, published experimental spectroscopic and theoretical molecular evidence of the identity of sulfate/selenate surface species are integrated with a surface complexation model consistent with a wide variety of experimental adsorption, surface titration, and proton coadsorption data to define the surface speciation of sulfate and selenate on iron oxides under a wide range of conditions. The analysis was carried out with the extended triple layer model (ETLM) taking into account the electrostatics of water dipole desorption during ligand exchange reactions. On seven out of eight goethites studied, sulfate and selenate surface reactions can be represented by the formation of a monodentate-mononuclear inner-sphere and a bidentate-binuclear outer-sphere (or H-bonded) species according to

$$> \mathrm{FeOH} + \mathrm{H^+} + \mathrm{AO_4^{2-}} => \mathrm{FeOAO_3^-} + \mathrm{H_2O}$$

and

$$> \mathrm{FeOH} + 2\mathrm{H^+} + \mathrm{AO_4^{2-}} = (> \mathrm{FeOH_2^+})_2\_\mathrm{AO_4^{2-}}$$

respectively, where A stands for S or Se. The model predicted changes in the proportions of the species with pH, ionic strength and surface coverage consistent with independently derived experimental evidence from *in situ* Raman, ATR-FTIR and EXAFS studies. In contrast to goethite, the ETLM analysis of sulfate and selenate adsorption on hydrous ferric oxide (HFO) required an additional outer-sphere (or H-bonded) surface species represented by,

$$> \mathrm{FeOH} + 2\mathrm{H^+} + \mathrm{AO_4^{2-}} => \mathrm{FeOH_2^+}\_\mathrm{HAO_4^-}$$

Equilibrium constants for sulfate and selenate adsorption based on site-occupancy standard states (K^0) for $> \mathrm{FeOAO_3^-}$ and $(> \mathrm{FeOH_2^+})_2\_\mathrm{AO_4^{2-}}$ on HFO are systematically higher than those on goethite, indicating that HFO has a greater affinity for sulfate and selenate than goethite.

1. Introduction

Sulfate is a common anionic species in natural aqueous systems from soils to the oceans. Adsorption of sulfate on iron oxides affects a variety of other geochemical processes. Sulfate adsorption competes with phosphate, carbonate and organic acid adsorption (Ali and Dzombak, 1996; Geelhoed et al., 1997; Liu et al., 1999; Wijnja and Schulthess,

* Corresponding author.
E-mail addresses: fukushi@kenroku.kanazawa-u.ac.jp (K. Fukushi), sver@jhu.edu (D.A. Sverjensky).
[1] Current address: Institute of Nature and Environmental Technology, Kanazawa University, Kakuma-machi, Kanazawa, Ishikawa 920-1192, Japan.

0016-7037/$ - see front matter © 2006 Elsevier Inc. All rights reserved.
doi:10.1016/j.gca.2006.08.048

2002). The presence of sulfate affects the adsorption of trace metals by forming ternary surface complexes (Davis and Leckie, 1978a,b; Ostergren et al., 2000; Elzinga et al., 2001; Swedlund and Webster, 2001; Swedlund et al., 2003). In addition, adsorption of sulfate enhances proton surface charge relative to monovalent anions such as chloride (Breeuwsma and Lyklema, 1973; Yates and Healy, 1975; Sigg and Stumm, 1980; Rietra et al., 1999), which strongly affects the adsorption behavior of other ions on mineral surfaces. To predict the migration of ionic species in natural systems, the adsorption behavior and the nature of adsorbed sulfate species on iron oxides must be known over the full range of environmental conditions.

Although selenate is a trace species in nature compared to sulfate, it is discussed here together with sulfate because the chemical characteristics of selenate are quite similar to sulfate (Balistrieri and Chao, 1990). In addition, selenium is an essential nutrient for humans and animals, it often accumulates in plants and can prove toxic to animals that ingest the vegetation (Peak and Sparks, 2002). Adsorption of selenate on iron oxides plays an important role in the distribution between solid and aqueous phases in natural environments (Balistrieri and Chao, 1990; Myneni et al., 1997; Wijnja and Schulthess, 2000; Peak and Sparks, 2002). Therefore, it is important to understand the adsorption behavior and nature of adsorbed selenate species on iron oxides over wide ranges of environmental conditions.

Evidence of the surface speciation of adsorbed sulfate and selenate on iron oxides has been obtained through infrared and X-ray spectroscopic studies, as well as theoretical molecular calculations. According to *in situ* ATR-FTIR spectroscopic investigations of sulfate adsorption on goethite as a function of pH, ionic strength and surface coverage (Peak et al., 1999; Wijnja and Schulthess, 2000), sulfate forms both inner-sphere and outer-sphere surface species on goethite, the relative proportions of which are functions mainly of pH and ionic strength. The inner-sphere complex was assigned to be a monodentate-mononuclear sulfate or bisulfate species. The bisulfate species has subsequently been ruled out by the application of MO/DFT calculations (Paul et al., 2005). The molecular calculations suggest that the ATR-FTIR results could be accounted for by a combination of monodentate-mononuclear inner-sphere plus a hydrogen-bonded sulfate species or a bidentate-binuclear inner-sphere species plus a hydrogen-bonded sulfate species. Distinguishing between a true outer-sphere complex (with waters of solvation associated with the sulfate) and a hydrogen-bonded complex may be difficult with MO/DFT calculations (Paul et al., 2005), nor is this difference explicitly treated in surface complexation models. In addition, aqueous phase IR studies of Fe(III)–sulfate interactions emphasize a different interpretation of the sulfate coordination compared to the surface IR studies cited above (Majzlan and Myneni, 2005). For the purposes of the present study, it is assumed that sulfate adsorption can be examined with an inner-sphere species and an additional species that may be either outer-sphere or hydrogen bonded to the surface. *In situ* ATR-IR studies of sulfate on hematite (Hug, 1997; Paul et al., 2005) are consistent with this approach, as are ATR-FTIR studies of selenate on goethite (Peak et al., 1999; Wijnja and Schulthess, 2000).

The nature of adsorbed selenate species has also been studied by X-ray absorption spectroscopy. An EXAFS study of selenate on goethite at pH 3.5 and 0.01 M $NaNO_3$ implied that selenate formed an outer-sphere species (Hayes et al., 1987; ionic strength given pers.comm. to the present authors). In contrast, it was concluded that selenate forms a bidentate-binuclear inner-sphere species on goethite and HFO, at pH values of 2.7–3.5 and 0.1 M $NaNO_3$ (Manceau and Charlet, 1994). It has been suggested that the apparent inconsistency between these results is a consequence of the difference in ionic strength in the experiments (Peak and Sparks, 2002). Calculations illustrating this difference are presented below using a surface complexation model of the selenate/goethite/water interface.

Surface complexation models of sulfate and selenate adsorption on iron oxides have been presented in numerous studies (Sigg and Stumm, 1980; Hayes et al., 1988; Balistrieri and Chao, 1990; Zhang and Sparks, 1990,; Ali and Dzombak, 1996; Geelhoed et al., 1997; Rietra et al., 1999; Rietra et al., 2001; Rahnemaie et al., 2006). However, the complexation reactions estimated from the regression of macroscopic adsorption data have not always been consistent with the more recent *in situ* spectroscopic data (Sigg and Stumm, 1980; Balistrieri and Chao, 1990; Zhang and Sparks, 1990; Ali and Dzombak, 1996). It has become widely recognized that the evidence of oxyanion speciation from spectroscopic studies should be integrated with models describing macroscopic adsorption data (Suarez et al., 1997; Hiemstra and van Riemsdijk, 1999; Blesa et al., 2000; Goldberg and Johnston, 2001).

A pioneering effort to integrate the spectroscopic evidence of oxyanion speciation with surface complexation is the charge-distribution (CD) model (Hiemstra and van Riemsdijk, 1996; Hiemstra and van Riemsdijk, 1999), according to which the charge of an adsorbed anion is split between two adsorption planes. The splitting factor (f) can be predicted from Pauling bond strength considerations when the coordination of the anion is established from spectroscopy. The factor f is then used to modify the electrostatic work of ion adsorption. In turn, this strongly affects the model calculations. In practice, f is often used as a fit parameter, in addition to the equilibrium constant for adsorption of the anion (Hiemstra and van Riemsdijk, 1996; Geelhoed et al., 1998; Rietra et al., 1999; Hiemstra and van Riemsdijk, 2000; Rietra et al., 2001; Antelo et al., 2005). As a consequence, the CD model loses sensitivity to alternative speciation schemes. For example, the CD model can fit sulfate and selenate adsorption data equally well with either an inner-sphere complex or both inner- and outer-sphere complexes (Rietra et al., 2001). In addition, for sulfate on goethite, the predicted proportions of the

two species as a function of ionic strength are not consistent with spectroscopic results (Rietra et al., 2001). A more recent CD model fit to the same sulfate data involved inner- and outer-sphere sulfate species with only three fit parameters, but did not address the issue of the predicted ionic strength dependence of the two species in comparison with ATR-FTIR trends (Rahnemaie et al., 2006).

An alternative approach, the dipole modification of the triple-layer model (ETLM, Sverjensky and Fukushi, 2006a) is capable of independently predicting the proportions of inner- and outer-sphere surface complexes as functions of pH, ionic strength, and surface coverage consistent with spectroscopic results. This is possible because the ETLM takes into account a previously neglected phenomenon integral to inner-sphere surface complexation reactions: the electrostatic work associated with desorption of the water dipoles in a ligan-exchange mechanism (Fig. 1). It has been shown that the magnitude of the electrostatic work associated with this dipole modification to the TLM is substantial and depends only on the stoichiometry of the surface reaction. No new fitting parameters are involved. The electrolyte and surface protonation part of the ETLM is the same as previously described (Sverjensky, 2005, 2006). As a result, the sensitivity of the ETLM to predicting alternate speciation schemes is enhanced. When the structures of adsorbed anions established in spectroscopic studies are used to calibrate models of bulk adsorption data, the models then independently predict the proportions of inner- to outer-sphere surface complexes as functions of pH, ionic strength and surface coverage. The predicted proportions compare very favorably with spectroscopic results for sulfate (SO_4^{2-}) on goethite, arsenite (AsO_3^{3-}) on β-$Al(OH)_3$, and oxalate ($C_2O_4^{2-}$) on goethite (Sverjensky and Fukushi, 2006a). For arsenite and oxalate the agreement is quantitative, for sulfate the spectroscopic data give qualitative trends only which agree with the model predictions. However, the applicability of the model to a wide variety of goethites synthesized under different conditions, and, to a wide variety of surface chemical measurements involving sulfate and selenate (e.g., isotherms, proton surface titration, proton coadsorption, and electrokinetic studies) has yet to be investigated.

In the present study, we demonstrate the applicability of the ETLM to a variety of surface chemical measurements involving sulfate and selenate on a wide range of goethites (Yates and Healy, 1975; Sigg and Stumm, 1980; Balistrieri and Murray, 1981; Hayes et al., 1988; Ali and Dzombak, 1996; Geelhoed et al., 1997; Liu et al., 1999; Rietra et al., 2001) and hydrous ferric oxide (HFO) (Davis and Leckie, 1980; Hayes et al., 1988; Balistrieri and Chao, 1990; Swedlund and Webster, 2001), including adsorption envelope, adsorption isotherms, proton surface titration in the presence of sulfate and selenate, proton coadsorption with sulfate and selenate, and electrokinetic studies. The purpose of the study is to determine the effect of pH, ionic strength,

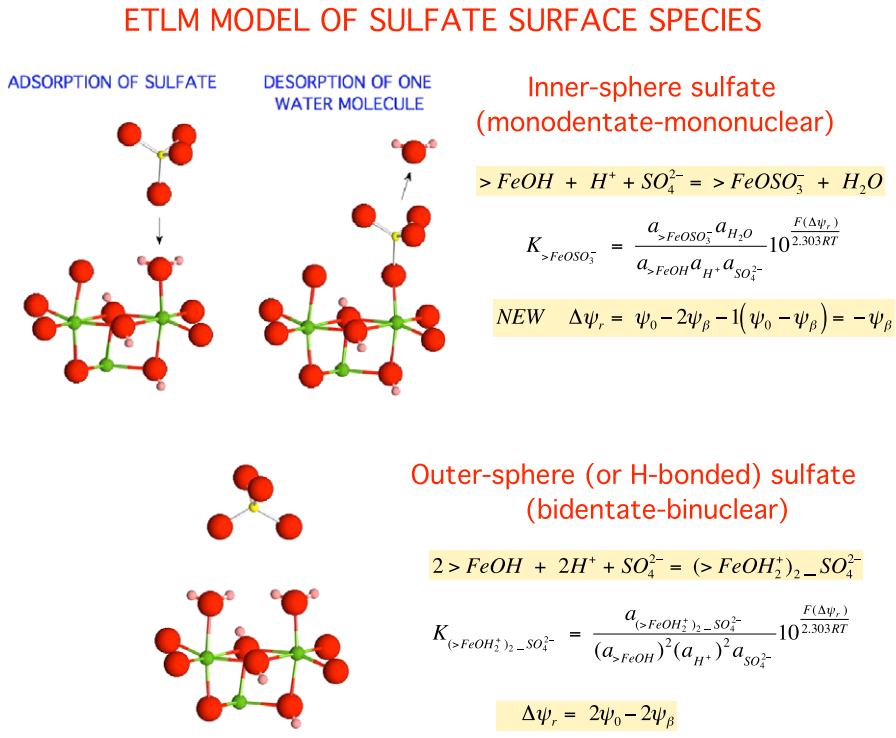

Fig. 1. Diagrammatic representations and model reactions of the formation of inner- and outer-sphere sulfate surface species according to the ETLM (Sverjensky and Fukushi, 2006a,b). The inner-sphere species forms by a ligand-exchange reaction which releases one water dipole. This effect is taken into account in the electrostatic term for the reaction ($\Delta\Psi_r$), which includes contributions from the ions and the water dipole. The outer-sphere (or H-bonded) sulfate surface species has an electrostatic term dependent only on the ions in the reaction.

surface coverage and type of adsorbant on the surface speciation of sulfate and selenate on iron oxides and to compare the results with trends established from FTIR and X-ray spectroscopic studies and evidence of possible speciation from theoretical molecular studies. In addition, the performance of the ETLM for integrating spectroscopic with bulk adsorption data is compared with the CD model.

2. ETLM treatment of sulfate/selenate adsorption

2.1. Aqueous speciation, surface protonation and electrolyte adsorption

Aqueous speciation calculations were carried out taking into account aqueous ionic activity coefficients appropriate to single electrolytes up to high ionic strengths calculated with the extended Debye–Huckel equation (Helgeson et al., 1981; Criscenti and Sverjensky, 1999). Electrolyte ion pairs used were consistent with previous studies (Criscenti and Sverjensky, 1999; Criscenti and Sverjensky, 2002). Aqueous sulfate and selenate protonation and aqueous complex equilibria are summarized in Table 1.

The sample characteristics and surface protonation and electrolyte adsorption equilibrium constants used in the present study are summarized in Table 2. Surface protonation constants referring to site-occupancy standard states (indicated by the superscript "θ",), i.e., $\log K_1^\theta$ and $\log K_2^\theta$, were calculated from values of pH_{ZPC} and ΔpK_n^θ (Sverjensky, 2005):

$$\log K_1^\theta = pH_{ZPC} - \frac{\Delta pK_n^\theta}{2} \quad (1)$$

$$\log K_2^\theta = pH_{ZPC} + \frac{\Delta pK_n^\theta}{2} \quad (2)$$

Values of pH_{ZPC} were taken from point-of-zero-salt effects or reported zero-point-of-charge by authors corrected for electrolyte adsorption (Sverjensky, 2005). For HFO examined by Hayes et al. (1988) and Swedlund and Webster (2001), neither isoelectric points nor surface titration data were reported. It was assumed that these HFO samples have the same $pH_{ZPC} = 7.9$ as in Davis and Leckie (1978a,b). Values of ΔpK_n^θ were predicted theoretically (Sverjensky, 2005). For convenience, equilibrium constants expressed relative to the hypothetical 1.0 molar standard state, (indicated by the superscript "0") as well as the equilibrium constants expressed relative to site-occupancy standard states, are given in Table 2. The relationships between the two standard states are given by

$$\log K_1^0 = \log K_1^\theta - \log\left(\frac{N_S A_S}{N^\ddagger A^\ddagger}\right) \quad (3)$$

$$\log K_2^0 = \log K_2^\theta + \log\left(\frac{N_S A_S}{N^\ddagger A^\ddagger}\right) \quad (4)$$

where,

N_S represents the surface site density on the sth solid sorbent (sites m^{-2})

$N^\ddagger$ represents the standard state sorbate species site density (sites m^{-2})

A_S represents the BET surface area of the sth solid sorbent ($m^2\ g^{-1}$)

$A^\ddagger$ represents a standard state BET surface area ($m^2\ g^{-1}$)

In the present study, values of $N^\ddagger = 10 \times 10^{18}$ sites m^{-2} and $A^\ddagger = 10\ m^2\ g^{-1}$ are selected for all solids.

Electrolyte adsorption equilibrium constants referring to site-occupancy standard states, $\log K_{M^+}^\theta$ and $\log K_{L^-}^\theta$, and capacitances, C_1, were obtained from regression of proton surface charge data when such data were available. In other instances, these parameters were obtained by theoretical prediction (Sverjensky, 2005) or from similar samples as noted in Table 2. For convenience, values for the hypothetical 1.0 molar standard state relative to >SOH species, $\log {}^*K_{M^+}^0$ and $\log {}^*K_{L^-}^0$ (where the superscript "*" represents a reaction relative to the species >SOH), are also given in Table 2. The relationships between $\log {}^*K_{M^+}^0$ and $\log {}^*K_{L^-}^0$, and $\log K_{M^+}^\theta$ and $\log K_{L^-}^\theta$ are given by

$$\log {}^*K_{M^+}^0 = \log K_{M^+}^\theta - pH_{ZPC} - \Delta pK_n^\theta - \log\left(\frac{N_S A_S}{N^\ddagger A^\ddagger}\right) \quad (5)$$

$$\log {}^*K_{L^-}^0 = \log K_{L^-}^\theta + pH_{ZPC} - \Delta pK_n^\theta - \log\left(\frac{N_S A_S}{N^\ddagger A^\ddagger}\right) \quad (6)$$

Surface areas of the iron oxides (A_S) were taken from experimental measurements where possible. For goethite, measured BET surface areas were used (Table 1). However, for samples of HFO, it was assumed that the surface areas are 600 $m^2\ g^{-1}$ as established in earlier studies (Davis and Leckie, 1978a,b; Dzombak and Morel, 1990).

Site densities (N_S) were derived from regression of oxyanion adsorption data as a function of surface coverage where these data were available. This procedure was adopted because oxyanions are likely to adsorb on only a subset of the total sites available (Hiemstra and van Riemsdijk, 1996, 1999; Catalano et al., 2006a,b) and because theoretical estimation of site densities is impossible for a powdered sample when the proportions of all the crystal faces are unknown. In most experimental studies, the latter information is not available. In addition, the surface chemical characteristics of goethites in general vary widely, even those synthesized in the absence of CO_2 (Sverjensky,

Table 1
Aqueous protonation and aqueous complex formation constants of sulfate and selenate at 25 °C used in present study

Reactions	log K	References
$HSO_4^- = SO_4^{2-} + H^+$	−1.98	[a]
$HSeO_4^- = SeO_4^{2-} + H^+$	−1.80	[b]
$NaSO_4^- = SO_4^{2-} + Na^+$	−0.88	[d]
$NaSeO_4^- = SeO_4^{2-} + Na^+$	−0.88	[d]
$KSO_4^- = SO_4^{2-} + K^+$	−0.88	[c]
$KSeO_4^- = SeO_4^{2-} + K^+$	−0.88	[d]

[a] Shock et al. (1997).
[b] Seby et al. (2001).
[c] Sverjensky et al. (1997).
[d] Assumed the same as the KSO_4^- species.

Table 2
Sample characteristics, surface protonation and electrolyte adsorption equilibrium constants, and capacitances used in present study

Solid	Salt (ml)	N_S[c] (sites nm^{-2})	A_S[d] (m^2 g^{-1})	pH_{ZPC}[e]	ΔpK_n^{θ}[f]	$\log K_1^{\theta}$	$\log K_2^{\theta}$	$\log {}^*K_1^0$	$\log {}^*K_2^0$	$\log K_M^{\theta}$	$\log K_L^{\theta}$	$\log {}^*K_M^0$	$\log {}^*K_L^0$	C_1 (μF cm^2)	Source of surface charge data	Adsorption data
Goethite	NaCl	2.5	79.4	8.0	5.6	5.2	10.8	4.9	−11.1	3.3	3.1	−7.8	8.0	115	Ali and Dzombak (1996)[i]	Ali and Dzombak (1996)
Goethite	$NaNO_3$	2.3	96.4	9.4	5.6	6.6	12.2	6.3	−12.5	3.0	2.7	−9.5	9.0	80	Rietra et al. (2000)[n]	Rietra et al. (1999a & 2001)
Goethite	KNO_3	2.3	96.4	9.4	5.6	6.6	12.2	6.3	−12.5	3.0	2.7	−9.5	9.0	80	Rietra et al. (2000)[n]	Geelhoed et al. (1997)
Goethite	KCl	3.0	82	7.8	5.6	5.0	10.6	4.6	−11.0	3.2[g]	3.2[g]	−7.8	7.8	125[g]	—[k]	Liu et al. (1999)
Goethite	KNO_3	3.6	48	7.5	5.6	4.7	10.3	4.5	−10.5	3.2	3.1	−7.3	7.6	65	Yates and Healy (1975)[l]	Yates and Healy (1975)
Goethite	$NaClO_4$	4.2	29	7.6	5.6	4.8	10.4	4.7	−10.5	3.4	2.4	−7.1	7.3	175	Sigg and Stumm (1980)[m]	Sigg and Stumm (1980)
Goethite	NaCl	3.5	52	7.6	5.6	4.8	10.4	4.5	−10.7	2.5	2.5	−8.2	7.0	90	Balistrieri and Murray (1981)[j]	Balistrieri and Murray (1981)
Goethite	$NaNO_3$	2.3	95	9.3	5.6	6.5	12.1	6.2	−12.4	3.5	3.2	−8.9	9.4	60	Venema et al. (1996)[i]	Rietra et al. (2001)
Goethite	$NaNO_3$	3.5	52	8.4	5.6	5.6	11.2	5.3	−11.5	3.2	3.3	−8.3	8.6	60	Hayes, 1987)[i]	Hayes et al. (1988)
HFO	$NaNO_3$	3.8	600	7.9	5.6	5.1	10.7	3.7	−12.1	4.3	4.5	−7.8	8.2	100	Davis and Leckie (1978a,b)[o]	Davis and Leckie (1978a,b)
HFO	$NaNO_3$	3.8	600	7.9	5.6	5.1	10.7	3.7	−12.1	4.3[h]	4.5[h]	−7.8	8.2	100[h]	Davis and Leckie (1978a,b)[o]	Swedlund and Webster (2001)
HFO	KCl	3.8	600	7.7	5.6	5.1	10.7	3.5	−11.9	4.3[h]	4.5[h]	−7.8	8.2	100[h]	Davis and Leckie (1978a,b)[o]	Balistrieri and Chao (1990)
HFO	$NaNO_3$	3.8	600	7.9	5.6	5.1	10.7	3.7	−12.1	4.3[h]	4.5[h]	−7.8	8.2	100[h]	Davis and Leckie (1978a,b)[o]	Hayes et al. (1988)

Values of $\log K_1^{\theta}$, $\log K_2^{\theta}$, $\log K_{M^+}^{\theta}$ and $\log K_{L^-}^{\theta}$ refer to site-occupancy standard states for the reactions listed below[a]. Values of $\log K_1^{\theta}$ and $\log K_2^{\theta}$, were predicted using the given values of pH_{ZPC} and ΔpK_n^{θ}. Values of $\log K_{M^+}^{\theta}$, $\log K_{L^-}^{\theta}$ and C_1 were estimated from regression of proton surface charge data unless otherwise noted. Values for $\log {}^*K_{M^+}^0$ and $\log {}^*K_{L^-}^0$ refer to the hypothetical 1.0 M standard state and the reactions listed below[b]. They were calculated from the values of $\log K_1^{\theta}$, $\log K_2^{\theta}$, $\log K_{M^+}^{\theta}$ and $\log K_{L^-}^{\theta}$ with the aid of Eqs. (3)–(6) using the tabulated values of N_S, A_S, pH_{ZPC} and ΔpK_n^{θ}.

[a] $\log K_1^{\theta}$: $> SOH + H^+ => SOH_2^+$; $\log K_2^{\theta}$: $>SO^- + H^+ = >SOH$; $\log K_{M^+}^{\theta}$: $>SO^- + M^+ = >SO^-\_M^+$; $\log K_{L^-}^{\theta}$: $> SOH_2^+ + L^- => SOH_2^+\_L^-$.

[b] $\log K_1^0$: $> SOH + H^+ => SOH_2^+$; $\log K_2^0$: $>SO^- + H^+ = >SOH$; $\log {}^*K_{M^+}^0$: $>SOH + M^+ = >SO^-\_M^+ + H^+$; $\log {}^*K_{L^-}^0$: $> SOH + H^+ + L^- => SOH_2^+\_L^-$.

[c] Values generated by regression of sulfate or selenate adsorption data as a function of surface coverage except for the goethites from Yates and Healy (1975), Sigg and Stumm (1980), Balistrieri and Murray (1981) and Hayes et al. (1988) which were predicted using the correlation with surface area in Fig. 5. Values for HFO were estimated from regression of arsenite adsorption data (Sverjensky and Fukushi, 2006b).

[d] Surface areas from BET measurements by the authors with the exception of HFO for which the surface area was taken from Davis and Leckie (1978a,b).

[e] Zero points of charge taken from point-of-zero-salt-effect or reported point of zero charge by authors corrected for electrolyte adsorption after Sverjensky (2005). The values for HFO by Swedlund and Webster (2001) and Hayes et al. (1988) were assumed to be the same as measured by Davis and Leckie (1978a,b).

[f] Predicted theoretically (Sverjensky, 2005).

[g] Predicted theoretically (Sverjensky, 2005).

[h] Assumed same as Davis and Leckie, 1978a,b.

[i] Sverjensky (2005).

[j] Sverjensky and Fukushi (2006a,b).

[k] Predicted theoretically (Sverjensky, 2005).

[l] Present study (see Fig. 3a).

[m] Present study (see Fig. 3c).

[n] Present study (see Fig. 4a).

[o] Criscenti and Sverjensky (2002).

2005). Together with site densities for goethites already published (Sverjensky and Fukushi, 2006a,b), the results of the present study define an empirical correlation between site density and surface area of goethite that enabled estimation of site densities for those goethites for which oxyanion adsorption data over a wide range of surface coverage were not available (see below). In the case of HFO samples, we used a single site density taken from our previous regression results for As(III) adsorption data (Sverjensky and Fukushi, 2006a,b).

For simplicity, we used a single site density for each sample applied to all the surface equilibria: oxyanion, surface protonation and electrolyte equilibria. This is possible because the predicted surface protonation and electrolyte adsorption equilibrium constants summarized previously (Sverjensky, 2005, 2006) refer to site-occupancy standard states independent of the site densities and surface areas of actual samples. They can be transformed to equilibrium constants referring to individual sample characteristics (e.g., the hypothetical 1.0 M standard states) using relationships such as Eqs. (3)–(6) above. For the sake of interest, we also tried analysing the oxyanion adsorption data using a two-site model, i.e., with different site densities for oxyanion adsorption versus proton (and electrolyte) adsorption, but did not obtain significantly different results. All the calculations reported here were carried out with the aid of the computer code GEOSURF (Sahai and Sverjensky, 1998). However, any code that treats a triple-layer model could also be used for the ETLM calculations reported below because the water dipole correction described below only affects how the electrostatic factor for inner-sphere oxyanion complexes is formulated.

2.2. Sulfate and selenate adsorption

In the ETLM treatment of sulfate and selenate adsorption on goethite, we investigated the applicability of the inner-sphere and outer-sphere (or H-bonded) complexes depicted in Fig. 1 (after Sverjensky and Fukushi, 2006a). The inner-sphere species is a monodentate-mononuclear species represented by

$$>\mathrm{FeOH} + \mathrm{H^+} + \mathrm{AO_4^{2-}} => \mathrm{FeOAO_3^-} + \mathrm{H_2O} \tag{7}$$

and

$${}^*K^{\theta}_{>\mathrm{FeOAO_3^-}} = \frac{a_{>\mathrm{FeOAO_3^-}} a_{\mathrm{H_2O}}}{a_{>\mathrm{FeOH}} a_{\mathrm{H^+}} a_{\mathrm{AO_4^{2-}}}} 10^{\frac{F(\Delta\Psi_r)}{2.303RT}} \tag{8}$$

where $\mathrm{AO_4^{2-}}$ represents S or Se. The outer-sphere species is represented by

$$2>\mathrm{FeOH} + 2\mathrm{H^+} + \mathrm{AO_4^{2-}} = (>\mathrm{FeOH_2^+})_2\_\mathrm{AO_4^{2-}} \tag{9}$$

and

$${}^*K^{\theta}_{(>\mathrm{FeOH_2^+})_2\_\mathrm{AO_4^{2-}}} = \frac{a_{(>\mathrm{FeOH_2^+})_2\_\mathrm{AO_4^{2-}}}}{a^2_{>\mathrm{FeOH}} a^2_{\mathrm{H^+}} a_{\mathrm{AO_4^{2-}}}} 10^{\frac{F(2\Psi_0 - 2\Psi_\beta)}{2.303RT}} \tag{10}$$

The relationships of the site-occupancy standard states to the hypothetical 1.0 M standard state are given by

$$\log {}^*K^{\theta}_{>\mathrm{FeOAO_3^-}} = \log {}^*K^{0}_{>\mathrm{FeOAO_3^-}} + \log\left(\frac{N_S A_S}{N^{\ddagger} A^{\ddagger}}\right) \tag{11}$$

$$\log {}^*K^{\theta}_{(>\mathrm{FeOH_2^+})_2\_\mathrm{AO_4^{2-}}} = \log {}^*K^{0}_{(>\mathrm{FeOH_2^+})_2\_\mathrm{AO_4^{2-}}} + \log\left(\frac{(N_S A_S)^2}{N^{\ddagger} A^{\ddagger}} C_S\right) \tag{12}$$

where C_S denotes solid concentration ($g\ L^{-1}$).

In the exponential term of Eq. (8), $\Delta\Psi_r$ represents the electrostatic factor related to the work done in an electric field when species in the reaction move on or off the charged surface. With the ETLM, $\Delta\Psi_r$ is evaluated taking into account the adsorbing ions and the water dipole released in Eq. (7) (Sverjensky and Fukushi, 2006a). The ions experience changes in potential relative to the bulk solution depending on which plane in the model they are placed. Similarly, the water molecule released, which is an electric dipole, must also experience a change in potential leaving the charged surface. Electrostatic work is done in the case of the ions and in the case of the water dipole.

We place the charge of the proton in Eq. (7) on the 0-plane and the charge of the sulfate/selenate on the β-plane. The latter is a departure from the practice advocated by Hayes et al. (1988), but because of the dipole modification, the ETLM produces the same overall result for $\Delta\Psi_r$ as recent studies (using the CD-TLM approach) of carbonate on goethite (Villalobos and Leckie, 2001; Villalobos et al., 2003) and arsenate on hematite (Arai et al., 2004). It should be emphasized here that an inner-sphere complex on the β-plane is reasonable because of the complexity of the distribution of oxide surface functional groups. The oxygens in these functional groups do not, in general, all lie on a single plane, but instead occur at different distances from the bulk lattice of the solid. For example, the terminal oxygen in >TiOH extends further out than the bridging oxygen in $>\mathrm{Ti_2O(H)}$ on the rutile (110) surface (Fenter et al., 2000; Zhang et al., 2004) and similarly for the terminal oxygen in >AlOH vs. the oxygen in $>\mathrm{Al_3O(H)}$ (Catalano et al., 2006a). Because the terminal >SOH groups are the ones most likely to participate in inner-sphere complexation with oxyanions (e.g., Hiemstra and van Riemsdijk, 1999; Catalano et al., 2006a,b), the potential experienced by the bound oxyanion can be envisioned as being well-approximated by the potential at the β-plane.

In the ETLM, the water dipole leaving the charged surface experiences a change in potential equal to $-n(\Psi_0 - \Psi_\beta)$ where n is the number of desorbed waters per reaction (Sverjensky and Fukushi, 2006a). For the reaction in Eq. (7), $n = 1$ so the ETLM results in

$$\Delta\Psi_r = \Psi_0 - 2\Psi_\beta - (\Psi_0 - \Psi_\beta) = -\Psi_\beta \tag{13}$$

For the outer-sphere complex in Eq. (10), we continue to express the electrostatic factor in the traditional way for

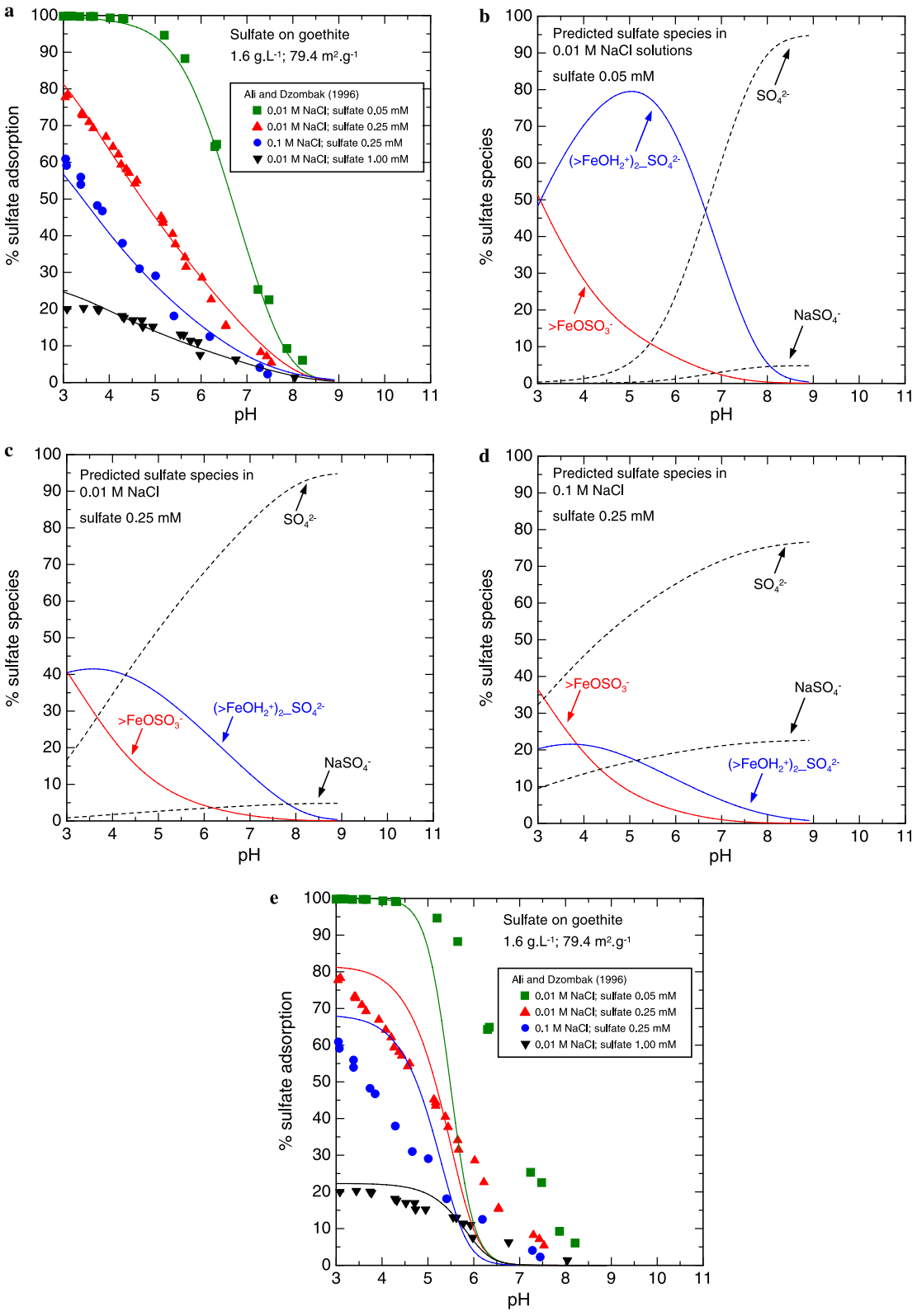

Fig. 2. The data points represent experimental results for sulfate adsorption on goethite from Ali and Dzombak (1996). The curves in (a) represent regression calculations but those in (b–d) represent predictions made with the ETLM using the sulfate surface species and parameters in Tables 2 and 3. (a) Sulfate adsorption as a function of pH, ionic strength and surface coverage. (b–d) Predicted sulfate speciation. The proportion of outer-sphere species is predicted to increase with pH, but decrease with ionic strength consistent with *in situ* ATR-FTIR results (Peak et al., 1999; Wijnja and Schulthess, 2000). (e) Regression of sulfate adsorption using an inner-sphere, bidentate-binuclear sulfate surface species (Eqs. (14)–(16)). The poor fit to the data indicates that such a species is not appropriate.

β-plane complexes in the triple-layer model (Davis and Leckie, 1980).

It can be seen in Fig. 2a that the combination of reactions (7) and (9) results in a close description of the experimental adsorption data over wide ranges of pH values, ionic strengths and surface coverages. The data shown in Fig. 2a cover such a wide range of conditions, including surface coverage, that they were used to regress for the two equilibrium constants and the site density. An independent test of the model can be made by comparison of model predictions with qualitative trends in ATR-FTIR spectroscopic results as pH, ionic strength and surface coverage are varied. It can be seen in Fig. 2b–d that the proportion of the outer-sphere complex is predicted to increase as a function of pH and decrease with ionic strength and surface coverage. All three of these predicted model variations were detected spectroscopically (Peak et al., 1999; Wijnja and Schulthess, 2000), which provides strong support for the ETLM for sulfate. Comparisons for selenate with X-ray absorption studies are discussed below. Finally, predicted values of the ξ-potential assuming that $\xi = \Psi_d$ indicate no significant shift with of the isoelectric point with sulfate loading, consistent with extrapolation of trends of experimental values of ξ-potential (Hansmann and Anderson, 1985).

Eqs. (7) and (9) are also consistent with the infrared and MO/DFT evidence for sulfate and selenate surface species summarized above. The monodentate-mononuclear inner-sphere sulfate species in Eq. (7), i.e., $>\mathrm{FeOSO_3^-}$, is supported by both the ATR-FTIR and molecular studies. Molecular studies (Paul et al., 2005) have also suggested that an alternate possibility is a bidentate-binuclear sulfate species, which could be represented by the reaction

$$2>\mathrm{FeOH} + 2\mathrm{H^+} + \mathrm{SO_4^{2-}} = (>\mathrm{FeO})_2\mathrm{SO_2^0} + 2\mathrm{H_2O} \quad (14)$$

and

$${}^*K^{\theta}_{(>\mathrm{FeO})_2\mathrm{SO_2^0}} = \frac{a_{(>\mathrm{FeO})_2\mathrm{SO_2^0}} a^2_{\mathrm{H_2O}}}{a^2_{>\mathrm{FeOH}} a^2_{\mathrm{H^+}} a_{\mathrm{SO_4^{2-}}}} 10^{\frac{F(\Delta\Psi_r)}{2.303RT}} \quad (15)$$

where

$$\Delta\Psi_r = 2\Psi_0 - 2\Psi_\beta - 2(\Psi_0 - \Psi_\beta) = 0 \quad (16)$$

because 2 mol of water are desorbed in Eq. (14). It can be seen in Fig. 2e that the reaction forming the bidentate-binuclear species provides a very poor fit to the bulk adsorption data. Consequently, the ETLM calculations suggest that this species is not a viable one. Instead, the two species discussed above, $>\mathrm{FeOSO_3^-}$ and $(>\mathrm{FeOH_2^+})_2\_\mathrm{SO_4^{2-}}$ are supported not only by ATR-FTIR studies and molecular calculations, but are also consistent with a surface complexation description of the bulk adsorption data from Ali and Dzombak (1996).

Even though the fitted curves in Fig. 2a provide a close description of the experimental adsorption data from Ali and Dzombak (1996), and the predicted model variations in Fig. 2b–d agree with the independently established trends from spectroscopy, it remains to be shown how applicable the model is for other goethites and other types of surface chemical measurements. Goethites synthesized under different conditions can have distinctly different surface properties (Sverjensky, 2005). Consequently, we investigate a wide variety of goethites in the calculations reported below. It has also been repeatedly emphasized in the literature that surface complexation models should be tested by application not just to adsorption edges, but also to isotherm measurements, proton surface titration in the presence of oxyanions, proton coadsorption with oxyanions, and electrokinetic studies (e.g., Rietra et al., 2001). A major purpose of the present paper is to investigate the applicability of the ETLM to a wide range of goethites and different types of surface chemical measurements.

For sulfate and selenate adsorption on hydrous ferric oxide (HFO), an additional outer-sphere (or H-bonded) species was needed to describe the adsorption data:

$$>\mathrm{FeOH} + 2\mathrm{H^+} + \mathrm{AO_4^{2-}} => \mathrm{FeOH_2^+}\_\mathrm{HAO_4^-} \quad (17)$$

$${}^*K^{\theta}_{>\mathrm{FeOH_2^+}\_\mathrm{HAO_4^-}} = \frac{a_{>\mathrm{FeOH_2^+}\_\mathrm{HAO_4^-}}}{a_{>\mathrm{FeOH}} a^2_{\mathrm{H^+}} a_{\mathrm{AO_4^{2-}}}} 10^{\frac{F(\Psi_0-\Psi_\beta)}{2.303RT}} \quad (18)$$

The relationship to the hypothetical 1.0 M standard state is given by

$$\log {}^*K^{\theta}_{>\mathrm{FeOH_2^+}\_\mathrm{HAO_4^-}} = \log {}^*K^{0}_{>\mathrm{FeOH_2^+}\_\mathrm{HAO_4^-}} + \log\left(\frac{N_S A_S}{N^{\ddagger} A^{\ddagger}}\right) \quad (19)$$

The addition of the reaction in Eq. (17) is not inconsistent with the spectroscopic results for sulfate or selenate adsorption on HFO summarized above. It will be shown below that for selenate adsorption on goethite by Hayes et al. (1988), the reaction in Eq. (17) is needed instead of the reaction in Eq. (9).

The equilibrium constants expressed relative to the species >SOH (using the superscript "*") in Eqs. (8), (10) and (15), depend on the $\mathrm{pH_{ZPC}}$ and $\Delta \mathrm{p}K_n^{\theta}$ of samples . The reported $\mathrm{pH_{ZPC}}$ of iron oxides significantly vary with experimental conditions. Therefore, it is convenient to correct for differences in the $\mathrm{pH_{ZPC}}$ and $\Delta \mathrm{p}K_n^{\theta}$ by eliminating the contributions of surface protonation from equilibrium constants. These conversions can be made with the following equations (Sverjensky, 2005):

$$\log K^{\theta}_{>\mathrm{FeOAO_3^-}} = -\log {}^*K^{\theta}_{>\mathrm{FeOAO_3^-}} - \mathrm{pH_{ZPC}} + \frac{\Delta \mathrm{p}K_n^{\theta}}{2} \quad (20)$$

$$\log K^{\theta}_{(>\mathrm{FeOH_2^+})_2\_\mathrm{AO_4^{2-}}} = -\log {}^*K^{\theta}_{(>\mathrm{FeOH_2^+})_2\_\mathrm{AO_4^{2-}}} - 2\mathrm{pH_{ZPC}} + \Delta \mathrm{p}K_n^{\theta} \quad (21)$$

$$\log K^{\theta}_{>\mathrm{FeOH_2^+}\_\mathrm{HAO_4^-}} = -\log {}^*K^{\theta}_{>\mathrm{FeOH_2^+}\_\mathrm{HAO_4^-}} - \mathrm{pH_{ZPC}} + \frac{\Delta \mathrm{p}K_n^{\theta}}{2} \quad (22)$$

The resultant values of $\log K^{\theta}_{>\mathrm{FeOAO_3^-}}$, $\log K^{\theta}_{(>\mathrm{FeOH_2^+})_2\_\mathrm{AO_4^{2-}}}$ and $\log K^{\theta}_{>\mathrm{FeOH_2^+}\_\mathrm{HAO_4^-}}$ are independent of the site density, surface area or solid concentration of the specific samples

as well as pH_{ZPC} and ΔpK_n^θ of iron oxides used in the experiments. Values of $\log {}^*K^0_{>FeOAO_3^-}$, $\log {}^*K^0_{(>FeOH_2^+)_2\_AO_4^{2-}}$ and $\log {}^*K^0_{>FeOH_2^+\_HAO_4^-}$ referring to the hypothetical 1.0 M standard state and reactions formed from >FeOH, as well as values of $\log K^\theta_{>FeOAO_3^-}$, $\log K^\theta_{>FeOH_2^+\_HAO_4^-}$ and $\log K^\theta_{(>FeOH_2^+)_2\_AO_4^{2-}}$ (referring to site-occupancy standard states) for sulfate and selenate adsorption reactions are summarized in Table 3.

3. Application to sulfate and selenate adsorption

3.1. Sulfate adsorption

3.1.1. Adsorption of sulfate on goethite from Geelhoed et al. (1997) and Rietra et al. (1999, 2001)

It can be seen in Fig. 3a–d that an unusually wide range of different types of experimental measurements are depicted, including proton surface titration in the presence of sulfate, proton coadsorption with sulfate, adsorption isotherms and adsorption edges. Furthermore, the two goethites represented by these experimental studies were synthesized extremely carefully in CO_2-free conditions by a consistent, well-described method in the same laboratory (Venema et al., 1996; Geelhoed et al., 1997; Rietra et al., 2000). Consequently, the high BET surface areas and high pH_{ZPC} values (9.3–9.4) of these goethites define what are probably the most useful goethite samples for retrieving surface complexation equilibrium constants. They refer purely to the system under investigation (e.g., no carbonate contamination effects). It will also be seen that these high surface area goethites represent an end-member for the carbonate-free goethites considered in the present study.

The solid curves in Fig. 3a–d represent regression calculations using the same reactions as in Fig. 1, i.e., involving the species $>FeOSO_3^-$ and $(>FeOH_2^+)_2\_SO_4^{2-}$. In these calculations, three regression parameters were used, the two equilibrium constants for the sulfate surface species and the site density. It can be seen that the calculated curves provide a close description of the bulk of the experimental data of all kinds. It can be seen in Fig. 3c and d that the model slightly overestimates the isotherm data for pH 3 and pH 8 and underestimates the adsorption edge at ionic strength 0.5. Unfortunately, uncertainties in the experimental data are not available, but the uncertainties in the logarithms of the two equilibrium constants for the species $>FeOSO_3^-$ and $(>FeOH_2^+)_2\_SO_4^{2-}$ are of the order of ± 0.2, which would certainly cover the discrepancies indicated in the figures. Overall, it can be concluded that the ETLM provides a reasonably satisfactory description of a very wide range of types of surface chemical data and environmental variables.

The unusually wide range of types of experimental data in Fig. 3 also permit a test of an alternative approach, placing the sulfate charge on the 0-plane as originally suggested by Hayes et al. (1988). Together with the dipole correction this results in $\Delta\Psi_r = -2\Psi_0 + \Psi_\beta$ (see also footnotes to Table 3). This approach is represented by the heavy dashed curve in Fig. 3a which is clearly inconsistent with the proton surface titration data in the presence of sulfate at both low and high pH values. Similar discrepancies for this approach are discussed below with respect to other proton surface titration and adsorption data.

The data in Fig. 3a–d have also been extensively analysed with the CD model (Geelhoed et al., 1997; Rietra et al., 1999; Rietra et al., 2001; Rahnemaie et al., 2006). A CD analysis using two surface species identified from spectroscopic studies is represented by the light dashed curves in Fig. 3a and c (taken from Figs. 2 and 3 in Rietra et al., 2001). The light dashed curves represent a CD calculation using inner- and outer-sphere complexes with the charge distribution as a fit parameter for each species. In other words, a total of four fit parameters were used, two equilibrium constants and two CD parameters. It was also established by Rietra et al. (2001) and Rahnemaie et al. (2006) that the data in Fig. 3a–d could be equally well-fit using only one (inner-sphere) sulfate species. In other words, the CD model cannot distinguish between the need for one or two sulfate surface species from the macroscopic data fitting alone without the spectroscopic evidence of two species. In addition, with the two surface species just discussed, the CD model apparently does not predict the correct trend of increasing outer-sphere species with decreasing ionic strength (Rietra et al., 2001).

It can be seen in Fig. 3a and c that two out of the four dashed curves representing the CD model fit the experimental data more closely than do the solid curves of the present study using the ETLM. However, this might well be expected given the use of four fit parameters for the CD model compared to three for the ETLM. In particular, the two CD fit parameters are a very powerful influence on the fitting. They multiply directly into the electrostatic work factor ($\Delta\Psi_r$) for the reactions which strongly enhances fitting ability. The latter is also almost certainly the reason for the insensitivity of the CD model to a one-species fit versus a two-species fit. In contrast, the ETLM approach requires the use of two surface species to fit the adsorption data. This can be seen in Figs. 2b–d and Fig. 3f, where the two sulfate surface species are important in different pH regimes. If only one species were used, the overall shape of the bulk adsorption curve would not fit the data. Of course two species is also what is required by the spectroscopic evidence. The ETLM fitting process is sensitive to the number of surface species because the electrostatic work factor ($\Delta\Psi_r$) in the ETLM is not a fit parameter. Finally, the fact that the ETLM can predict the correct trend of sulfate surface speciation with ionic strength (e.g., Fig. 2c and d) is extremely useful.

The predicted model speciation of sulfate on goethite for isotherm data at a pH of 5.0 from Fig. 3c and for adsorption envelope data for low ionic strength from Fig. 3d are shown in Fig. 3e and f, respectively. Fig. 3e shows that the inner-sphere species increases in importance at high surface coverage at pH 5, which is consistent with qualitative

Table 3
Equilibrium constants for sulfate and selenate adsorption on goethite and HFO from regression of the data in Figs. 2–11

Solid	Adsorbate	$\log {}^{*}K^{0}_{>FeOAO_3^-}$	$\log K^{\theta}_{>FeOAO_3^-}$	$\log {}^{*}K^{0}_{>FeOH_2^+\_HAO_4^-}$	$\log K^{\theta}_{>FeOH_2^+\_HAO_4^-}$	C_S (g L^{-1})	$\log {}^{*}K^{0}_{(>FeOH_2^+)_2\_AO_4^{2-}}$	$\log K^{\theta}_{(>FeOH_2^+)_2\_AO_4^{2-}}$	Source	Data
Goethite	Sulfate	9.1	4.2	—	—	1.6	21.6	14.0	Ali and Dzombak (1996)	Fig. 2
Goethite	Sulfate	9.7	3.4	—	—	10	22.6	13.1	Rietra et al. (1999a & 2001)	Fig. 3a[c] and b
Goethite	Sulfate	9.7	3.4	—	—	20.6	22.3	13.1	Rietra et al. (2001)	Fig. 3c
Goethite	Sulfate	9.7	3.4	—	—	3.1	23.1	13.1	Rietra et al. (2001)	Fig. 3c
Goethite	Sulfate	9.7	3.4	—	—	0.5	23.9	13.1	Geelhoed et al. (1997)	Fig. 3d
Goethite	Sulfate	9.7	3.4	—	—	4	23.0	13.1	Geelhoed et al. (1997)	Fig. 3d and f
Goethite	Sulfate	9.6	5.0	—	—	1.064	21.8	14.6	Liu et al. (1999)	Fig. 4a–d
Goethite	Sulfate	9.3	4.8	—	—	4.17	19.8	13.5	Yates and Healy (1975)	Fig. 6a–b
Goethite	Sulfate	9.9	5.2	—	—	4.6	20.2	13.4	Sigg and Stumm (1980)	Fig. 6c–d[d]
Goethite	Sulfate	8.2	3.7	—	—	7.46	19.2	13.0	Balistrieri and Murray (1981)	Fig. 6e and f
HFO	Sulfate	10.2	6.5	16.5	12.8	0.088	—	—	Davis and Leckie (1978a,b)	Fig. 7a and b
HFO	Sulfate	11.5	7.8	—	—	0.0845	—	—	Swedlund and Webster (2001)	Fig. 7c and d
Goethite	Selenate	10.2	4.0	—	—	16.42	22.0	12.9	Rietra et al. (2001)	Fig. 8a and b
Goethite	Selenate	10.1	3.8	—	—	20.6	22.1	12.9	Rietra et al. (2001)	Fig. 8c
Goethite	Selenate	10.1	3.8	—	—	3.1	22.9	12.9	Rietra et al. (2001)	Fig. 8c
Goethite	Selenate	10.1	3.8	—	—	9.7	22.4	12.9	Rietra et al. (2001)	Fig. 8c and d
Goethite	Selenate	10.1	3.8	—	—	10	22.4	12.9	Rietra et al. (1999a & 2001)	Fig. 8e and f
Goethite	Selenate	10.1	3.8	—	—	30	21.9	12.9	Rietra et al. (2001)	Fig. 10c and d
Goethite	Selenate	9.8	4.4	16.6	11.3	30	—	—	Hayes et al. (1988)	Fig. 9a and c
Goethite	Selenate	9.8	4.4	16.6	11.3	3	—	—	Hayes et al. (1988)	Figs. 9b and d & 10a and b
HFO	Selenate	9.3	5.6	16.9	13.2	0.088	22.4	15.9	Davis and Leckie (1978a,b)	Fig. 11a and b
HFO	Selenate	9.6	6.1	16.8	13.3	0.0264	21.5	14.8	Balistrieri and Chao (1990)	Fig. 11c
HFO	Selenate	9.6	6.1	16.8	13.3	0.264	20.5	14.8	Balistrieri and Chao (1990)	Fig. 11c and d
HFO	Selenate	10.5	6.8	15.8	12.1	0.088	20.4	13.9	Hayes et al. (1988)	Fig. 11e and f

Values of $\log {}^{*}K^{0}_{>FeOAO_3^-}$, $\log {}^{*}K^{0}_{>FeOH_2^+\_HAO_4^-}$ and $\log {}^{*}K^{0}_{(>FeOH_2^+)_2\_AO_4^{2-}}$ refer to the hypothetical 1.0 M standard state and reactions formed form >FeOH[a]. Values of $\log K^{\theta}_{>FeOAO_3^-}$, $\log K^{\theta}_{>FeOH_2^+\_HAO_4^-}$ and $\log K^{\theta}_{(>FeOH_2^+)_2\_AO_4^{2-}}$ refer to site-occupancy standard states for sulfate and selenate adsorption reactions[b] calculated from the values of $\log {}^{*}K^{0}_{>FeOAO_3^-}$, $\log {}^{*}K^{0}_{>FeOH_2^+\_HAO_4^-}$ and $\log {}^{*}K^{0}_{(>FeOH_2^+)_2\_AO_4^{2-}}$ with aid of Eqs. (11), (12), (16), (17), (18) and (19) using values of N_S, A_S, pH_{ZPC} and ΔpK^{θ}_{n} from Table 2 and C_S from Table 3.

[a] $\log {}^{*}K^{0}_{>FeOAO_3^-}$: $> FeOH + H^+ + AO_4^{2-} => FeOAO_3^-$; $\log {}^{*}K^{0}_{>FeOH_2^+\_HAO_4^-}$: $> FeOH + 2H^+ + AO_4^{2-} => FeOH_2^+\_HAO_4^-$; $\log {}^{*}K^{0}_{(>FeOH_2^+)_2\_AO_4^{2-}}$: $2 > FeOH + 2H^+ + AO_4^{2-} = (> FeOH_2^+)_2\_AO_4^{2-}$.

[b] $\log K^{\theta}_{>FeOAO_3^-}$: $> FeOH_2^+ + AO_4^{2-} => FeOAO_3^-$; $\log K^{\theta}_{>FeOH_2^+\_HAO_4^-}$: $> FeOH_2^+ + H^+ + AO_4^{2-} => FeOH_2^+\_HAO_4^-$; $\log K^{\theta}_{(>FeOH_2^+)_2\_AO_4^{2-}}$: $2 > FeOH_2^+ + AO_4^{2-} = (> FeOH_2^+)_2\_AO_4^{2-}$.

[c] The heavy dashed curve is computed with $\Delta\Psi_r = -2\Psi_0 + \Psi_\beta$ for $> FeOSO_3^-$ and $\Delta\Psi_r = 2\Psi_0 - 2\Psi_\beta$ for $(> FeOH_2^+)_2\_SO_4^{2-}$. Values for $\log {}^{*}K^{0}_{>FeOAO_3^-}$ and $\log {}^{*}K^{0}_{>FeOH_2^+\_HAO_4^-}$ are -0.5 and 24.5, respectively.

[d] The heavy dashed curves are computed with $\Delta\Psi_r = -2\Psi_0 + \Psi_\beta$for $> FeOSO_3^-$ and $\Delta\Psi_r = 2\Psi_0 - 2\Psi_\beta$ for $(> FeOH_2^+)_2\_SO_4^{2-}$. Values for $\log {}^{*}K^{0}_{>FeOAO_3^-}$ and $\log {}^{*}K^{0}_{>FeOH_2^+\_HAO_4^-}$ are 3.0 and 20.7, respectively.

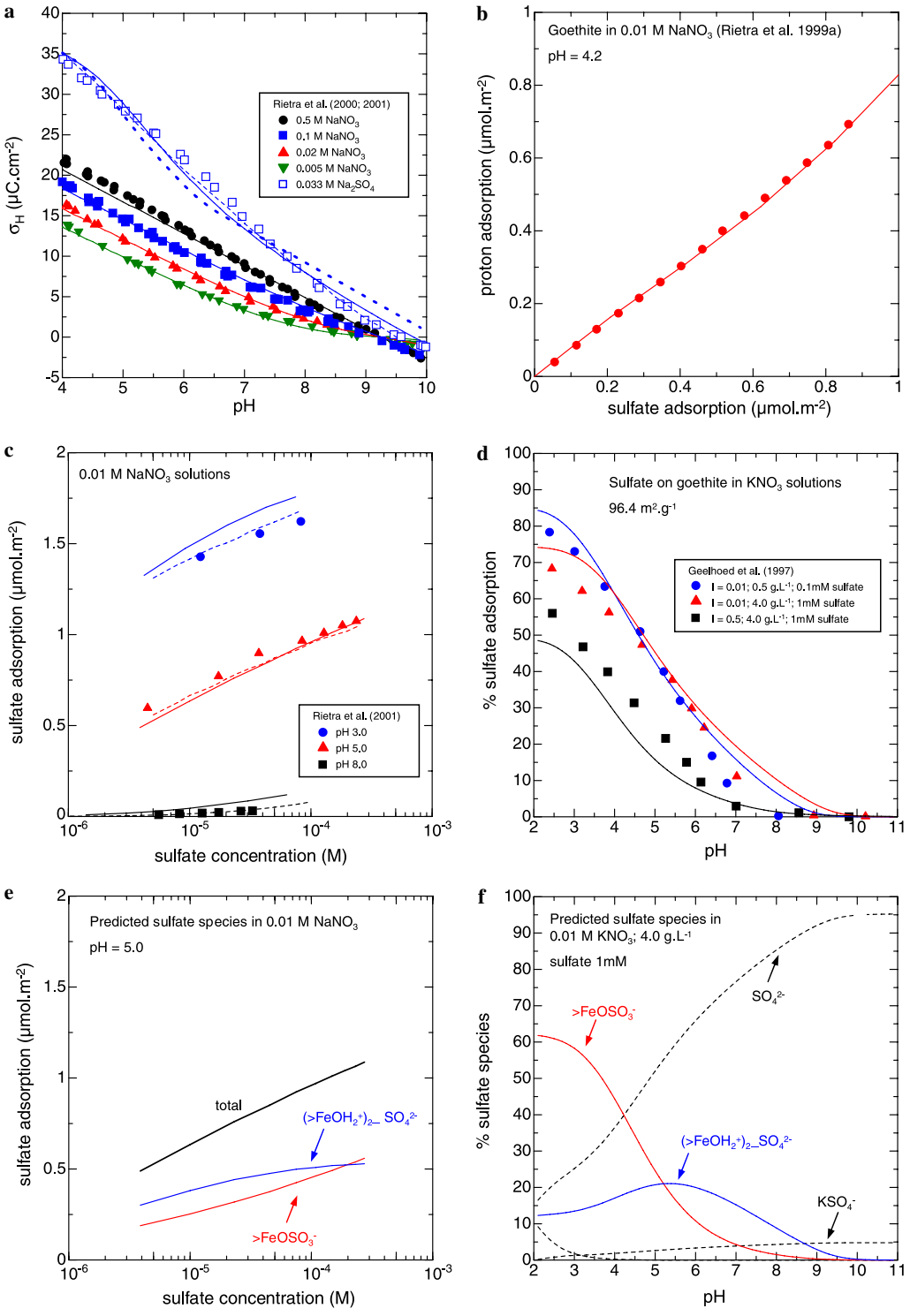

Fig. 3. The data points represent experimental results for sulfate adsorption on goethite from Rietra et al. (2001) and Geelhoed et al. (1997). The solid curves in (a–d) represent regression calculations with the ETLM using the two sulfate surface species and parameters in Tables 2 and 3. Three regression parameters were used, the two equilibrium constants and the site density. The curves in (e and f) represent predictions. The heavy dashed curve in (a) represents calculations with an alternate approach putting the charge of the sulfate on the 0-plane (see text and Table 3 footnotes). The light dashed curves in (a and c) represent a two-species, four parameter regression fit with the CD model (Rietra et al., 2001). (a) Proton surface charge as a function of pH and ionic strength in $NaNO_3$ and Na_2SO_4 electrolyte solutions. (b) Proton coadsorption with sulfate. (c) Sulfate adsorption as a function of pH and sulfate loading. (d) Sulfate adsorption as a function of pH, ionic strength and surface coverage. (e) Predicted sulfate speciation at pH 5 in (c). The proportion of outer-sphere species to inner-sphere species decreases with surface coverage, consistent with *in situ* ATR-FTIR results (Wijnja and Schulthess, 2000) at near neutral pH values. (f) Predicted sulfate speciation at $I = 0.01$ and 1mM of sulfate from Fig. 3d.

trends from FTIR spectroscopy as a function of sulfate loading at approximately pH 5.5 (Wijnja and Schulthess, 2000), as is the predicted trend with surface loading at near neutral pH. Fig. 3f compared to Fig. 2b–d shows that the inner-sphere species can predominate up to a pH of 5 at high enough surface loadings.

3.1.2. Adsorption of sulfate on goethite from Liu et al. (1999)

Regression calculations are depicted for adsorption edge and isotherm data from Liu et al. (1999) in Fig. 4a and c. Although the data are less extensive than those depicted in Figs. 2 and 3, the isotherm data again permit evaluation of the site density together with the equilibrium constants for the two sulfate surface species (Fig. 1). It can be seen that the calculated isotherm curve can reproduce the experimental data for the whole range of surface loading. This contrasts with ETLM analyses of As(III) adsorption on oxides where the model systematically underestimates the amount of adsorbed As(III) at high surface loading, which was attributed to surface precipitation or polymerization (Sverjensky and Fukushi, 2006b). The present results indicate that sulfate does not undergo precipitation or polymerization on goethite surfaces even at high surface loading.

The predicted model speciation of sulfate on goethite for the adsorption edge and isotherm conditions from Liu et al. (1999) can be seen in Fig. 4b and d. As discussed above for the other goethite studied here, it can be seen in Fig. 4b that the inner-sphere sulfate species dominates at low pH (here less than 4), but at higher pH values the outer-sphere (or H-bonded species)

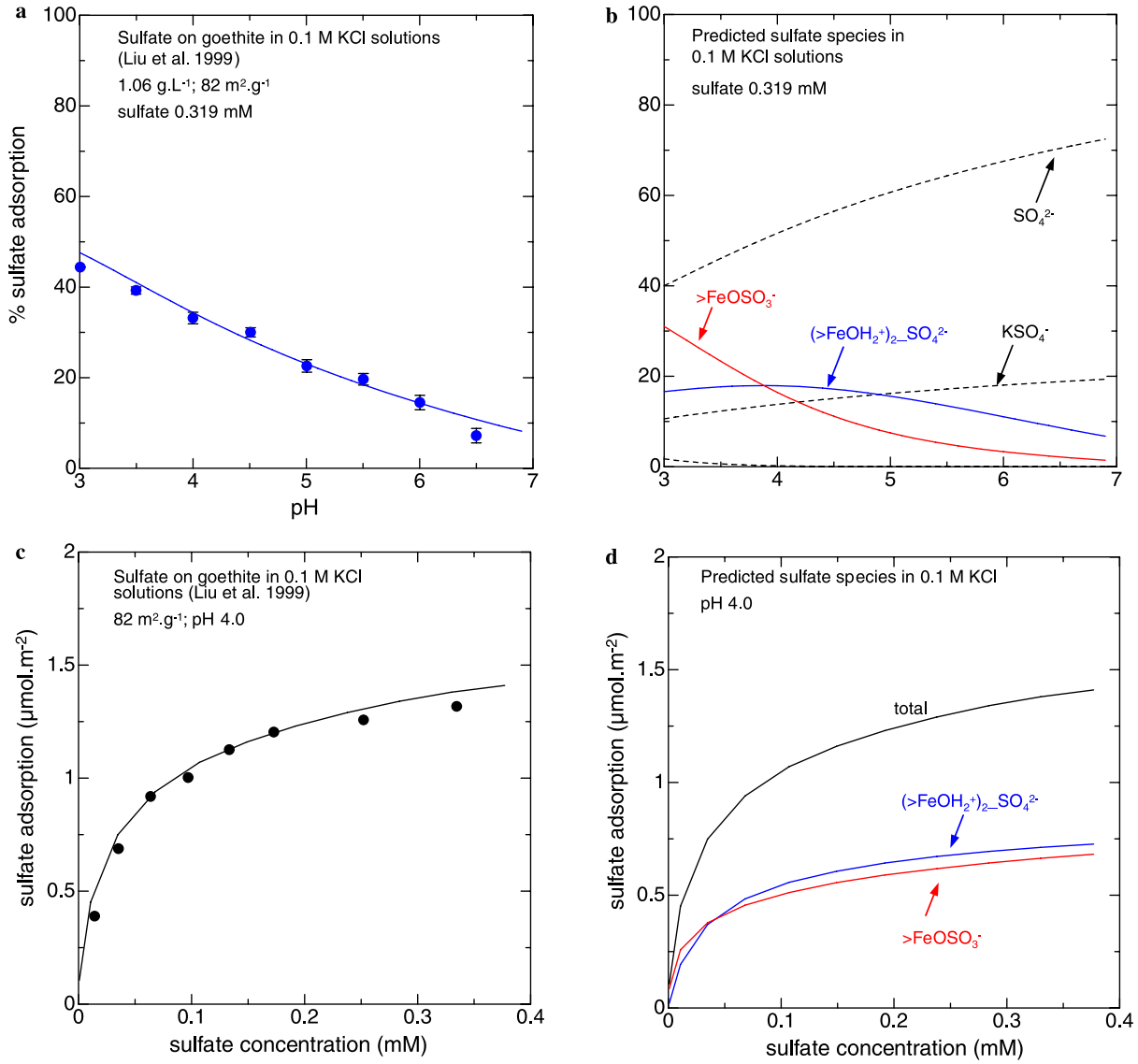

Fig. 4. The data points represent experimental results for sulfate adsorption on goethite from Liu et al. (1999). The curves in (a and c) represent regression calculations with the ETLM using the sulfate surface species and parameters in Tables 2 and 3. (a) Sulfate adsorption as a function of pH. (b) Predicted sulfate speciation in (a). (c) Sulfate adsorption as a function of sulfate loading. (d) Predicted sulfate speciation in (c). The proportion of outer-sphere species to inner-sphere species do not significantly change with surface coverage consistent with *in situ* ATR-IR results at low pH values (Peak et al., 1999).

predominates. Little difference is apparent in the proportion of the two sulfate surface species with surface loading (Fig. 4d), which is consistent with observations at pH 3.5 from ATR-FTIR spectroscopy (Peak et al., 1999).

3.1.3. Correlation of site densities with surface area for goethites

The regression calculations summarized above for sulfate on three goethites referring to adsorption data covering a wide range of surface coverages permitted simultaneous retrieval of equilibrium constants and site densities (Tables 2 and 3). The values of the site densities obtained are 2.5, 2.3, and 3.0 (±0.3) sites nm^{-2}, for goethites from Ali and Dzombak (1996), Rietra et al. (2001) and Liu et al. (1999), respectively. Such values compare favorably with the theoretical site density for singly coordinated oxygens, a value of 3.03 sites nm^{-2} for the (101) plane of goethite in the Pnma spacegroup (Gaboriaud and Erhardt, 2003) and the value for the same type of site on goethite powder (3.45 sites nm^{-2}, Hiemstra and van Riemsdijk, 1996).

Together with site densities obtained previously for other oxyanions on goethite (Sverjensky and Fukushi, 2006a,b), the results of the present study strongly suggest that there is a useful predictive relationship between site density and surface area for goethites. The data are plotted in Fig. 5 where it can be seen that there is a strong correlation. The same suggestion has already been made by Villalobos et al. (2003) based on an analysis of carbonate adsorption on goethites with widely different surface areas. The correlation in Fig. 5 could be the result of very different crystal faces or steps being exposed on the particles with different surface areas. However, a similar negative correlation between the capacitance C_1 and surface area for goethite (Sverjensky, 2005) suggests that the surface chemistry of goethites is more complex than this and requires further experimental characterization. From a practical standpoint the results depicted in Fig. 5 provide a useful tool for the estimation of site densities when adsorption data over a wide range of surface coverages is unavailable. We use this correlation for several of the goethites analyzed next in the present study.

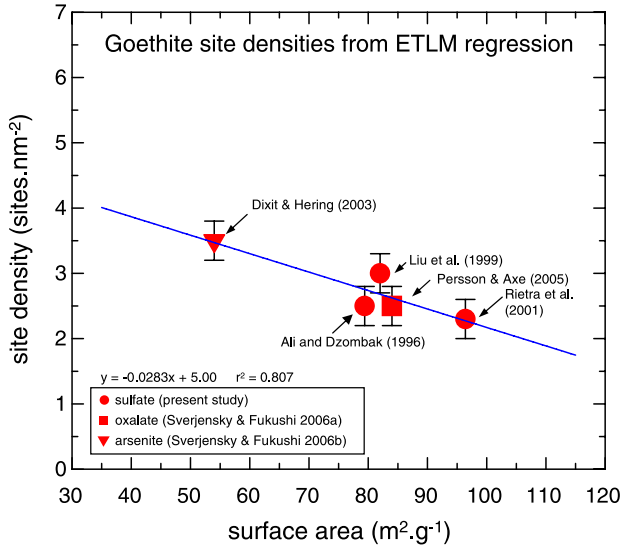

Fig. 5. Empirical correlation of goethite site densities generated with the ETLM by regression of adsorption data referring to a wide range of surface coverages for a range of different oxyanions. The line has a negative slope consistent with the results obtained for carbonate on goethites with different surface areas by Villalobos et al. (2003).

3.2. Adsorption of sulfate on goethite from Yates and Healy (1975), Sigg and Stumm (1980) and Balistrieri and Murray (1981)

As in Fig. 3a–d, it can be seen in Fig. 6a–e that both proton surface titration data in the presence of sulfate as well as sulfate adsorption data are depicted. However the three goethites referred to in Fig. 6a–e were probably not synthesized under CO_2-free conditions (Sigg and Stumm, 1980; Yates and Healy, 1975). Consequently, these goethites have very low pH_{ZPC} values (7.5 to 7.8). Retrieval of equilibrium constants for sulfate adsorption from these samples can be expected to be affected by carbonate contamination. Nevertheless, the solid curves in Fig. 6a–e represent regression calculations using the same reactions involving the species $>FeOSO_3^-$ and $(>FeOH_2^+)_2\_SO_4^{2-}$ used previously with site densities predicted from the correlation with surface area in Fig. 5. It can be seen that the calculated curves provide a close description of the bulk of the experimental data except at the extremes of pH.

We have also used the proton surface titration (and adsorption) data in Fig. 6c and d to test the alternative approach of placing the sulfate charge on the 0-plane, as described above for Fig. 3a (together with the dipole correction resulting in $\Delta\Psi_r = -2\Psi_0 + \Psi_\beta$ for the inner-sphere species, see footnotes to Table 3). This approach is represented by the heavy dashed curves in Fig. 6c and d which are clearly inconsistent with the data, particularly at lower pH values where the inner-sphere sulfate species predominates.

Returning to the ETLM calculations represented by the solid curves in Fig. 6a–d, it is interesting to compare the values of the equilibrium constants referring to the site-occupancy standard states for sulfate adsorption on these goethites with the values derived above for the CO_2-free conditions from the data in Fig. 3a–d. It can be seen in Table 3 that the values of $\log K^{\theta}_{(>FeOH_2^+)_2\_SO_4^{2-}}$ are 13.5, 13.4, and 13.0 for the Yates and Healy (1975), Sigg and Stumm (1980), and Balistrieri and Murray (1981) goethites, respectively, which agree within an overall uncertainty of ±0.3, and also agrees with the value of 13.1 for the goethites studied by Rietra et al. However, the corresponding values of $\log K^{\theta}_{>FeSO_3^-}$ are 4.8, 5.2, and 3.7, respectively, which do not agree well with each other, and two of them strongly disagree with the value of 3.4 for the Rietra et al. goethites.

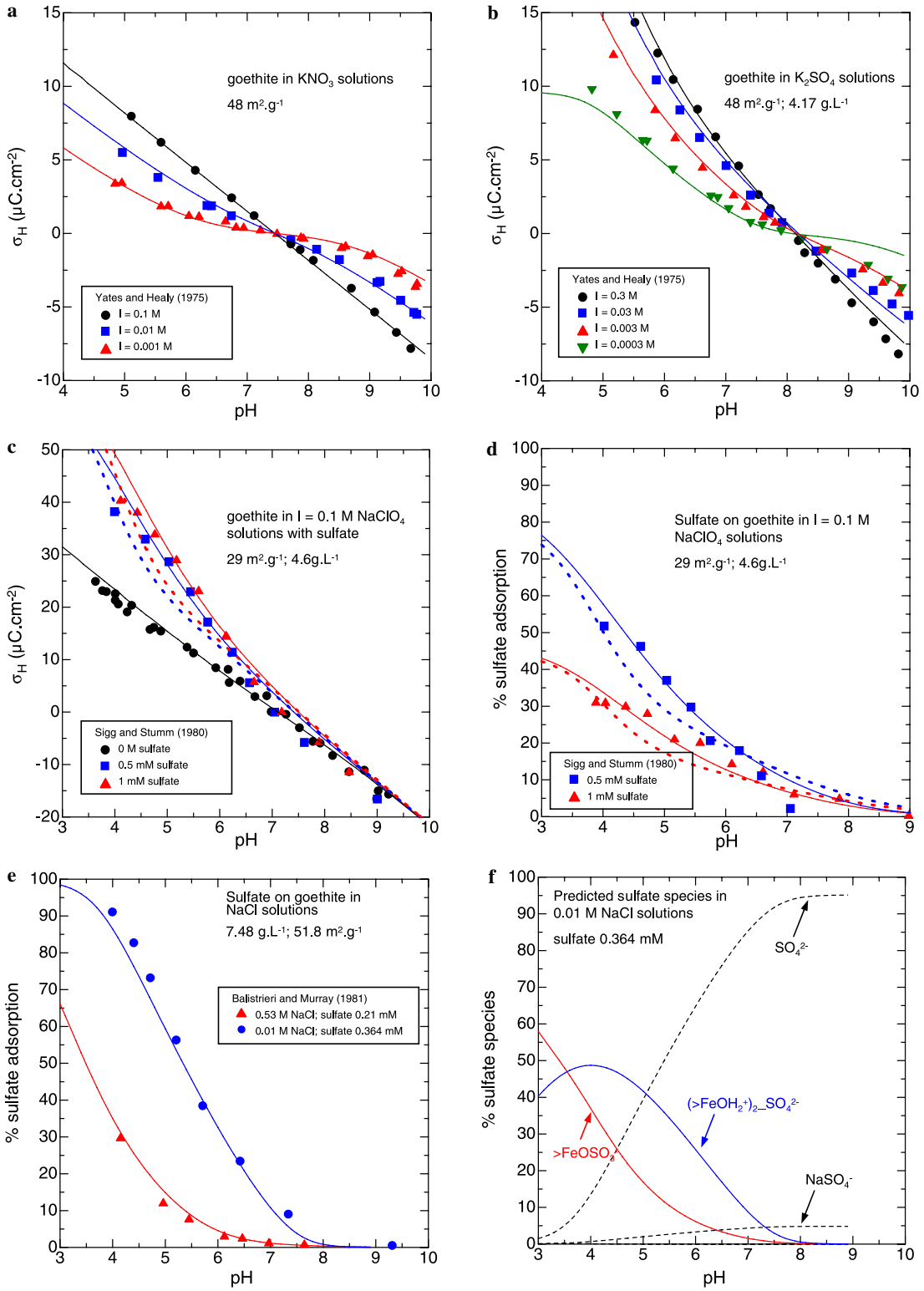

Fig. 6. The data points represent experimental results for sulfate adsorption on goethite from Yates and Healy (1975), Sigg and Stumm (1980) and Balistrieri and Murray (1981). The solid curves represent regression calculations with the ETLM using the sulfate surface species and parameters in Tables 2 and 3. The curves in (f) represent predictions. The heavy dashed curve in (c and d) represent calculations with an alternate approach putting the charge of the sulfate on the 0-plane (see text and Table 3 footnotes). (a and b) Proton surface titration as a function of pH and ionic strength in KNO_3 (a) and K_2SO_4 (b) electrolyte solutions. (c) Proton surface titration as a function of pH and sulfate concentration in $NaClO_4$ solutions. (d) Sulfate adsorption as a function of pH and surface coverage. (e) Sulfate adsorption as a function of pH and ionic strength. (f) Predicted sulfate speciation in Fig. 5e.

These values indicate that the effects of carbonate contamination affect the inner-sphere species more strongly, causing them to be anomalously large. This may be a consequence of the strong binding of carbonate as an inner-sphere species on goethite (Bargar et al., 2005).

The predicted model speciation of sulfate on the Balistrieri and Murray (1981) goethite is shown in Fig. 6f for the low ionic strength studied. It can again be seen that the monodentate inner-sphere species is predicted to predominate at pH less than 4 and the outer-sphere (or H-bonded) species becomes dominant at pH 4 to 8. The trends in surface speciation with pH are consistent with infrared spectroscopic results (Peak et al., 1999).

3.2.1. Adsorption of sulfate on HFO from Davis and Leckie (1980) and Swedlund and Webster (2001)

In contrast to all the above figures, the adsorption data depicted in Fig. 7a and c refer to adsorption of sulfate on HFO (Davis and Leckie, 1980; Swedlund and Webster, 2001). The solid lines in Fig. 7a refer to regression calculations using the same inner-sphere species as for sulfate on goethite (i.e., $>FeSO_4^-$). However, the data from Davis and Leckie (1980) required a different outer-sphere (or H-bonded) species, $>FeOH_2^+\_HSO_4^-$. It will be shown below that this type of species is also necessary for selenate adsorption on HFO, indicating a significant difference between the surface chemistry of HFO

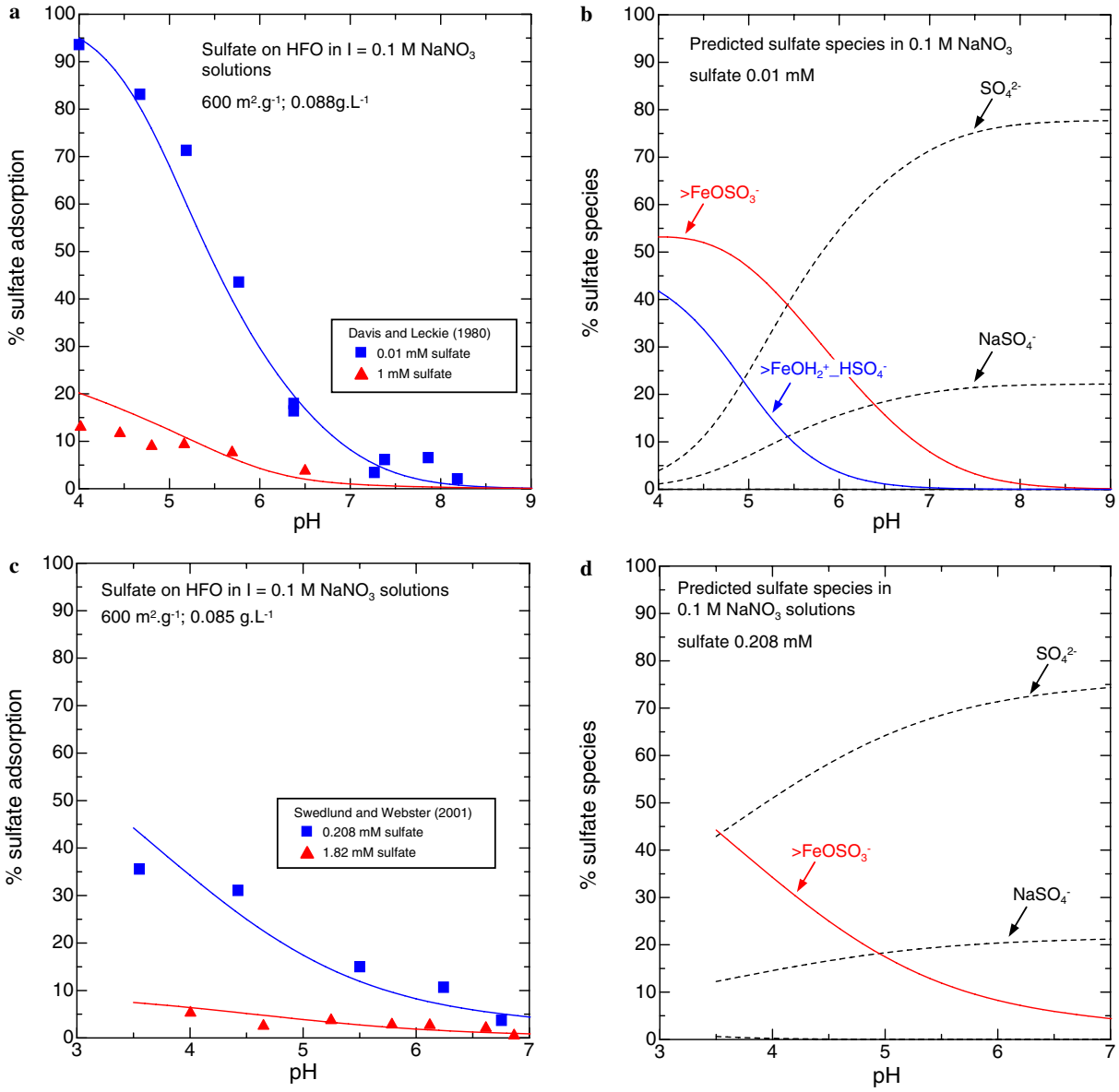

Fig. 7. The data points represent experimental results for sulfate adsorption on HFO from Davis and Leckie (1980) and Swedlund and Webster (2001). The curves in (a and c) represent regression calculations with the ETLM using the sulfate surface species and parameters in Tables 2 and 3. (a) Sulfate adsorption as a function of pH and sulfate loading. (b) Predicted sulfate speciation at 0.01mM of sulfate from (a). (c) Sulfate adsorption as a function of pH and sulfate loading. (d) Predicted sulfate speciation at 0.208 mM of sulfate from (c).

and most, but not all, goethites (the only goethite where this species appears in our analysis is from Hayes et al. discussed below). The solid lines in Fig. 7c, refer to only the inner-sphere sulfate surface complex, because the data are not sufficiently varied to require more than one surface species. An additional uncertainty in the calculations depicted in Fig. 7c is that the surface protonation and electrolyte adsorption characteristics of this sample are assumed to be the same as those established previously for the sample in Fig. 7a.

It can be seen in Table 3 that the values of $\log K^{\theta}_{>FeSO_3^-}$ for the two HFO samples in Fig. 7 are 6.5 (Davis and Leckie, 1980) and 7.8 (Swedlund and Webster, 2001). Although these values are not close in magnitude, which may well be a consequence of differences in sample history which have been neglected here or the simplicity of the speciation treatment for the Swedland and Webster sample. The values are significantly larger than the values for sulfate on carbonate-free goethite discussed above (e.g., 3.4 for the Rietra et al. samples). Larger equilibrium adsorption constants for sulfate on HFO relative to goethite are consistent with recent applications of Born solvation theory to arsenite adsorption on a variety of iron oxides (Sverjensky and Fukushi, 2006b). The larger $\log K^{\theta}_{>FeSO_3^-}$ values for HFO result from the larger dielectric constant of HFO. Under these circumstances, the work involved for dehydrating the adsorbing sulfate is negligible for the HFO-water interface, but for the goethite–water interface is large enough to be a significant influence opposing sulfate adsorption. Knowing the dielectric constants of other oxides suggests that it might be possible to make preliminary estimates of the values of $\log K^{\theta}_{>FeSO_3^-}$ for other oxides.

3.3. Selenate adsorption and surface speciation on iron oxides

3.3.1. Adsorption of selenate on goethite from Rietra et al. (1999, 2001)

A comprehensive study of selenate adsorption including proton surface titration in the presence of selenate, proton coadsorption with selenate, adsorption isotherms and adsorption edges is represented by the data depicted in Fig. 8a, c, e, and f (Rietra et al., 1999; Rietra et al., 2001). Furthermore, as in Fig. 3, the goethites used in these experimental studies represent CO_2-free conditions (Venema et al., 1996; Rietra et al., 1999). The solid curves in Fig. 8a, c, e, and f represent regression calculations using the same reaction stoichiometries as in Fig. 3, i.e., involving the species $>FeOSeO_3^-$ and $(>FeOH_2^+)_2{-}SeO_4^{2-}$, but in these calculations the site density was fixed at the value determined above for sulfate on the same goethite. Consequently, the only regression parameters were the two equilibrium constants. The selenate species used are also consistent with *in situ* Raman and ATR-FTIR results (Wijnja and Schulthess, 2000; Peak and Sparks, 2002). It can be seen that the calculated curves provide a close description of the bulk of the experimental data of all kinds. This also indicates that the site density we obtained for sulfate is applicable to selenate. Overall, it can be concluded that the ETLM provides a satisfactory description of a very wide range of types of surface chemical data and environmental variables, particularly when it is considered that only two fitting parameters (the two equilibrium constants) were involved. The fact that two selenate surface species are needed in this implementation of the ETLM can again be seen in the predicted selenate surface speciation plot (Fig. 8b). The two species occupy such different pH regimes that the sum of both is essential for describing the bulk adsorption data.

As in the case of sulfate discussed above, the same selenate data have been extensively analysed with the CD model in the studies where these data were originally published. A CD analysis using two surface species identified from spectroscopic studies is represented by the dashed curves in Fig. 8a, c, and e (taken from Figs. 1, 3, and 5 in Rietra et al., 2001). Dashed curves are given for only one isotherm in Fig. 8c to illustrate the maximum discrepancy between the CD and ETLM calculations. The dashed curves represent the same type of CD calculation as for sulfate, i.e., inner- and outer-sphere complexes with the charge distribution as a fit parameter for each species (i.e., four fit parameters: two equilibrium constants and two CD parameters). As for sulfate, the data in Fig. 8a, c, e, and f could be equally well-fit using only one (inner-sphere) selenate species. The CD model could not distinguish between the need for one or two selenate surface species from the macroscopic data fitting alone. It can be seen in Fig. 8a, c, e, and f that the dashed curves representing the CD model fit the experimental data more closely than do the solid curves using the ETLM. Again, this might well be expected given the use of four fit parameters for the CD model compared to two for the ETLM. Overall, the differences in the fits of the two sets of calculations do not seem significant.

A key set of data emphasized in the application of the CD model (Rietra et al., 1999) is the proton coadsorption data depicted in Fig. 8f for both selenate and sulfate. In order to adequately describe the small but significant difference between the proton coadsorption of selenate and sulfate, the CD model required not only different equilibrium constants but also different fitted charge distribution parameters, even when two surface species (i.e., inner- and outer-sphere) were used for both selenate and sulfate. In contrast, it can be seen here that the ETLM can describe the higher proton coadsorption with selenate relative to sulfate just with the equilibrium constants (i.e., a total of four fitting parameters, all of which are equilibrium constants). From an interpretive standpoint, the CD approach attributes the difference of proton coadsorption stoichiometry between selenate and sulfate to a difference in charge distribution at the interface, whereas the ETLM attributes the proton coadsorption difference to differences in the proportions of inner- and outer-sphere (or H-bonded) species.

A predicted model speciation of selenate on goethite is shown in Fig. 8b referring to low ionic strength

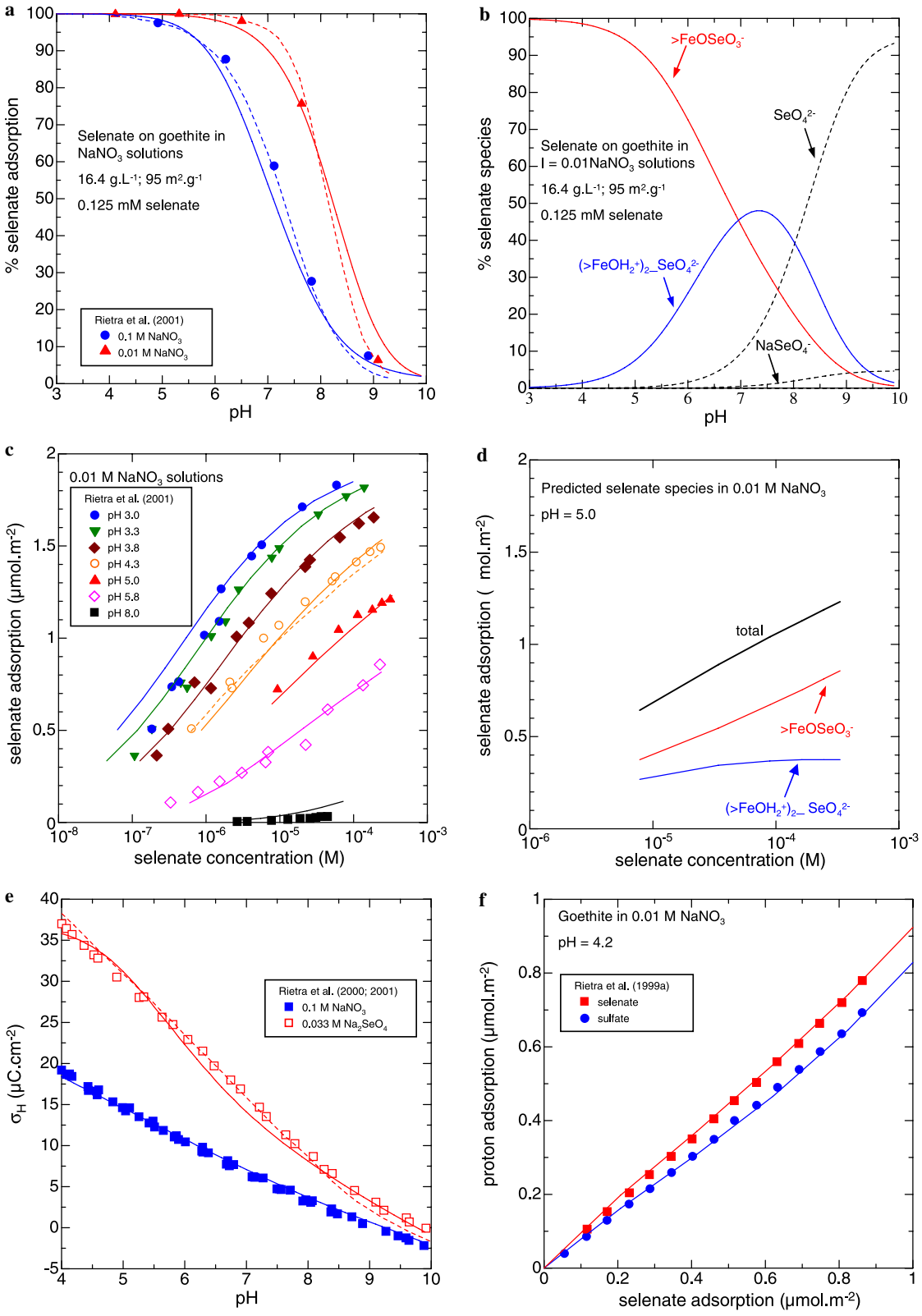

Fig. 8. The data points represent experimental results for selenate adsorption on goethite from Rietra et al. (1999, 2001). The solid curves in (a, c, e, and f) represent regression calculations with the ETLM using the surface species and parameters in Tables 2 and 3. The dashed curves in (a, c, and e) represent a two-species, four parameter regression fit with the CD model (Rietra et al., 2001). (a) Selenate adsorption on goethite synthesized by Venema et al. (1996) as a function of pH and ionic strength. The curves represent regression fits of experimental data plotted as symbols. (b) Predicted selenate speciation at $I = 0.01$ from (a and c) Selenate adsorption as a function of pH and selenate loading. (d) Predicted selenate speciation at pH 5 from (c). (e) Comparison of proton surface titration for Na_2SeO_4 and Na_2SO_4 electrolyte solutions. (f) Comparison of proton coadsorption with selenate and sulfate loading.

($I = 0.01$). It can be seen in Fig. 8b that the species $> FeOSeO_3^-$ is predicted to predominate at acidic conditions where the pH is less than 6.5, whereas the species $(> FeOH_2^+)_2\_SeO_4^{2-}$ is predicted to become dominant at pH values 7 to 9. This independently predicted trend of changes in surface speciation with pH is consistent with spectroscopic results (Rietra et al., 1999; Wijnja and Schulthess, 2000). It is also interesting to note that the dominant conditions for the outer-sphere or H-bonded selenate species is shifted to higher pH values compared with sulfate (see Fig. 3f). The predicted model selenate speciation for the adsorption isotherm is shown in Fig. 8d. Under the conditions shown, it can again be seen that the importance of the inner-sphere selenate species is enhanced when compared with sulfate adsorption under the same experimental conditions (see Fig. 3e). These features are also quantitatively expressed in the $\log K^{\theta}$ values derived in the present study, i.e., the $\log K^{\theta}_{>FeSeO_3^-}$ is higher than $\log K^{\theta}_{>FeSO_3^-}$ but $\log K^{\theta}_{(>FeOH_2^+)_2\_SeO_4^{2-}}$ is lower than $\log K^{\theta}_{(>FeOH_2^+)_2\_SO_4^{2-}}$.

3.3.2. Adsorption of selenate on goethite from Hayes et al. (1988)

The data depicted in Fig. 9a and b cover a very wide range of pH values, ionic strengths and an order of magnitude in surface coverage (Hayes et al., 1988). However, the goethite used in these experiments is very different to the ones used in Fig. 8. It has a significantly lower pH_{ZPC} value (8.4 compared with 9.3–9.4, Table 2), indicating that it is probably contaminated with CO_2. It can also be seen in Table 2 that the BET surface area of the goethite used by Hayes et al. (1988) is much lower than

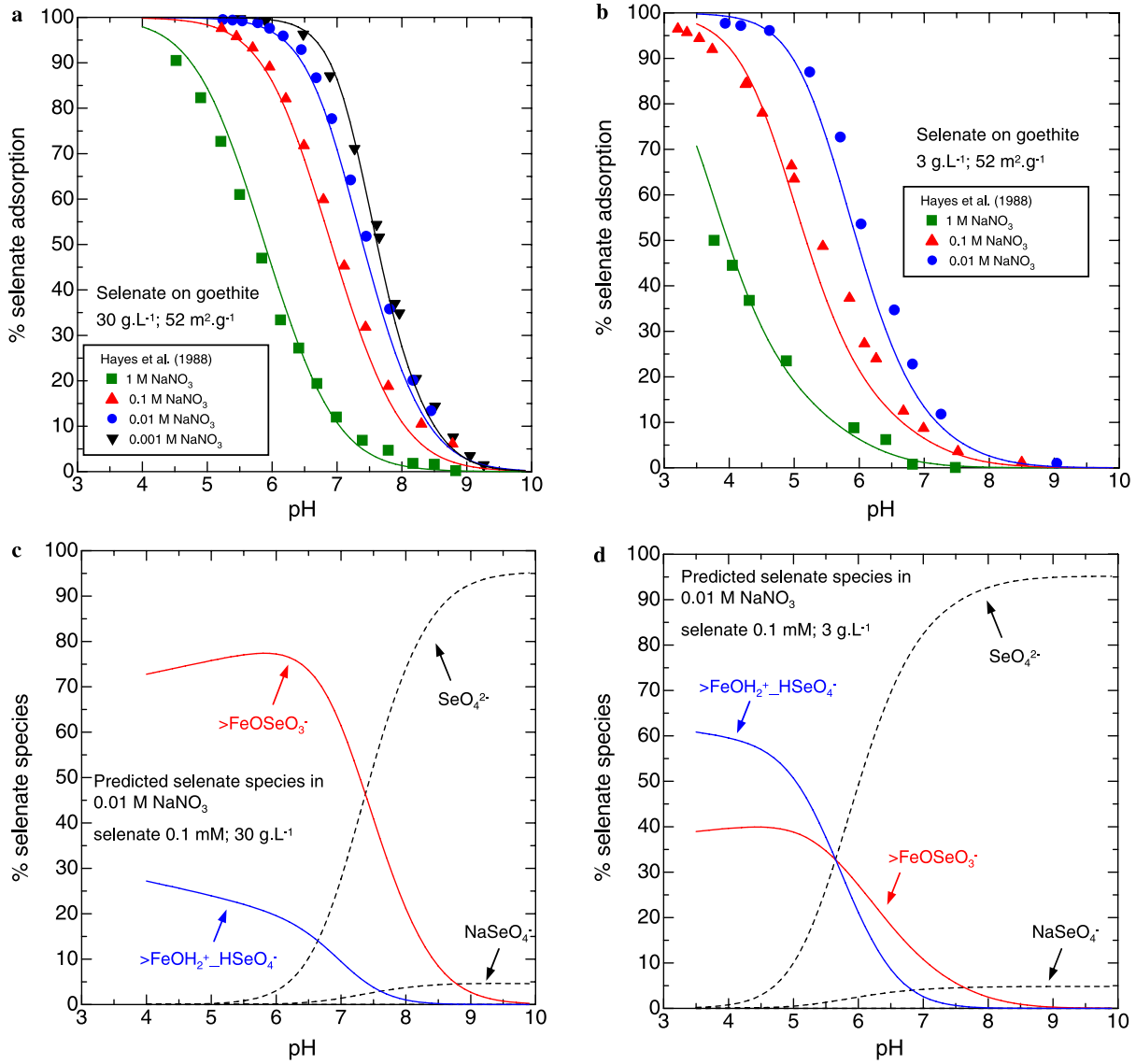

Fig. 9. The data points represent experimental results for selenate adsorption on goethite from Hayes et al. (1988). The curves in (a and b) represent regression calculations with the ETLM using the selenate surface species and parameters in Tables 2 and 3. (a and b) Selenate adsorption on goethite as a function of pH, ionic strength and surface coverage. Total selenate is 0.1 mM. (c and d) Predicted selenate speciation at $I = 0.01$ and 30 and 3 g L^{-1} from (a and b), respectively. The importance of the outer-sphere species increases with increasing surface coverage.

those used by Rietra et al. In addition, and in contrast to all the other goethites considered above for either sulfate or selenate adsorption, the surface species $>FeOSeO_3^-$ and, surprisingly, $>FeOH_2^+\_HSeO_4^-$, were discovered to be essential in the regression calculations, particularly for the higher surface coverages depicted in Fig. 9b. It can be seen in Fig. 9a and b that the calculated curves using these two selenate surface species provide close descriptions of the adsorption data over very wide ranges of conditions.

Although the reaction stoichiometry for the species $>FeOSeO_3^-$ is common to all the calculations for sulfate and selenate adsorption on goethite, the species $>FeOH_2^+\_HSeO_4^-$ has a stoichiometry not previously discovered for any of the other sulfate/selenate/goethite systems described above, which include seven different samples of goethite. In this regard the goethite studied by Hayes et al. appears to be anomalous. In fact surface species with the stoichiometry $>FeOH_2^+\_HSeO_4^-$ or $>FeOH_2^+\_HSO_4^-$ only otherwise seem to be associated with HFO samples, as noted above for Fig. 7a and b (and see also below for selenate/HFO). The anomalous behavior of Hayes et al.'s goethite suggests perhaps that the surface characteristics of this sample are, at least in part due to HFO mixed with the goethite. Although the Hayes et al. sample was checked with X-ray diffraction and goethite was detected (Hayes, 1987), amorphous HFO would be difficult to detect by this means.

The predicted model speciation of selenate for the adsorption envelopes are depicted in Fig. 9c and d. Speciation plots are given for low and high surface coverage at $I = 0.01$. It can be seen in Fig. 9c that for the relatively low surface coverage shown, the species $>FeOSeO_3^-$ is dominant at all pH values. However, at the higher surface coverage depicted in Fig. 9d, both selenate surface species are comparably abundant over a wide range of pH values. This result differs significantly from the results apparent in Fig. 8d referring to the high pH_{ZPC}, high BET, CO_2-free goethite studied by Rietra et al. Again, this emphasizes the anomalous nature of the goethite studied by Hayes et al. (1988).

3.3.3. Comparison of predicted ETLM selenate/goethite speciation with EXAFS results: Hayes et al. (1987) vs. Manceau and Charlet (1994)

As noted earlier, two EXAFS studies of selenate on goethite under similar acidic conditions have yielded apparently conflicting results. At a pH of 3.5, one study implied that selenate formed an outer-sphere species on goethite (Hayes et al., 1987). In contrast, at similar pH values of 2.7–3.5, it was concluded that selenate forms a bidentate-binuclear inner-sphere species on goethite and HFO (Manceau and Charlet, 1994). It is now clear, particularly from ATR-FTIR studies that selenate and sulfate, and probably most oxyanions, have two or more surface species on any given mineral and that the proportions of these species vary with environmental conditions (see also the ETLM calculations given above). Consequently, it has been suggested that the apparent inconsistency between the two EXAFS studies for selenate/goethite under acidic conditions is a consequence of the difference in ionic strength in the experiments leading to different surface speciations (Peak and Sparks, 2002). The ionic strength used in the Hayes et al. (1987) study was 0.01 (Hayes pers. comm.), whereas that in the Manceau and Charlet (1994) study was 0.1. The two also differ in surface coverage, because very high selenium concentrations are apparent in Fig. 10a (see Fig. 9a as well). Calculations illustrating these differences are presented below using the ETLM.

Model predictions of selenate surface speciation are given for the two different sets of EXAFS experiments (n.b. ionic strengths and surface coverages) in Fig. 10a and b. In each case, the calculations refer to the surface chemical characterization established for the (anomalous) goethite of Hayes et al. that was obtained above (Fig. 9, Tables 2 and 3). In the calculations, the species $>FeOSeO_3^-$ represents an inner-sphere species and $>FeOH_2^+\_HSeO_4^-$ represents what the EXAFS studies have termed an outer-sphere species. It can clearly be seen in Fig. 10a and b that a dramatic difference in the proportions of $>FeOSeO_3^-$ vs. $>FeOH_2^+\_HSeO_4^-$ is predicted for the two sets of EXAFS experiments. In Fig. 10a, at pH 3.5, $>FeOH_2^+\_HSeO_4^-$ is predicted to be more than two times abundant as $>FeOSeO_3^-$. The main reason for this is the much higher selenium concentrations in the Hayes et al. EXAFS system compared to the system used for the bulk adsorption studies (c.f. Fig. 9c). In contrast, in Fig. 10b, at pH values of about 3, $>FeOSeO_3^-$ is predicted to be almost twice as abundant as $>FeOH_2^+\_HSeO_4^-$. Although the level of sensitivity of the EXAFS experiments to the detection of minor amounts of inner-sphere species is rather uncertain, the model predictions in Fig. 10a and b certainly support the notion (Peak and Sparks, 2002) that differences in the adsorption conditions could account for the apparent disagreement between the results of the two EXAFS studies.

One difference between the results in Fig. 10b and the EXAFS results reported by Manceau and Charlet (1994) is that our model inner-sphere species is monodentate-mononuclear, whereas these researchers reported a Fe–Se distance consistent with a bidentate-binuclear inner-sphere species. The reason for this remaining discrepancy between calculation and experiment is not clear. However, the diverse nature of different types of solid reported as goethite has been emphasized repeatedly in this paper. Consequently, our use of the Hayes anomalous goethite surface chemical properties in the calculations shown in Fig. 10b, even though they refer to the environmental conditions described by Manceau and Charlet (1994), may be inappropriate. Unfortunately, the surface chemical properties of the specific goethite studied by Manceau and Charlet (1994) were not reported. An additional

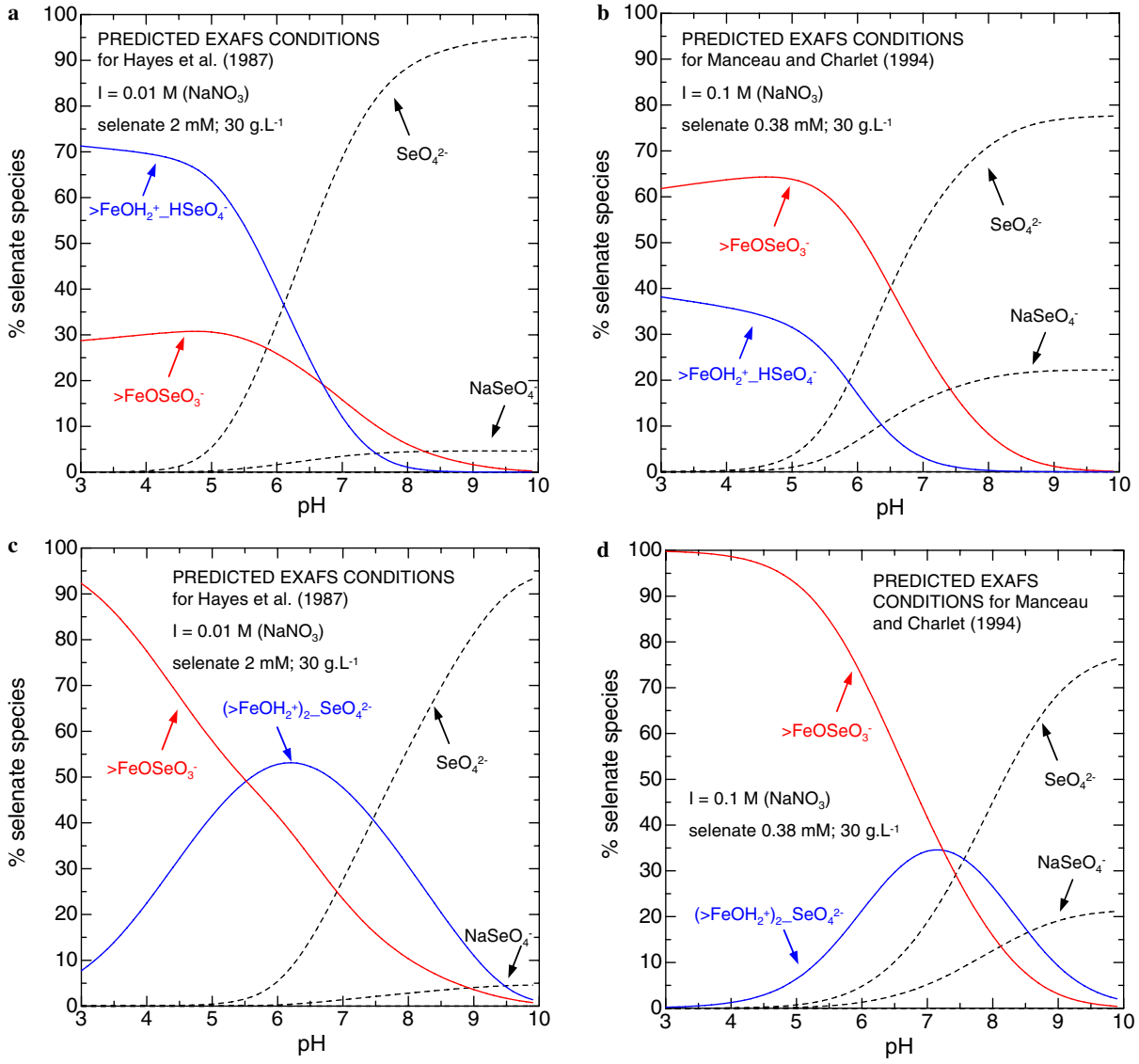

Fig. 10. Prediction of selenate surface speciation on goethite for the EXAFS conditions of Hayes et al. (1987) and Manceau and Charlet (1994). The curves in (a and b) represent predictions using the selenate surface species and parameters corresponding to the goethite from Hayes et al. (1988) given in Tables 2 and 3. The curves in (c and d) represent predictions using the selenate surface species and parameters corresponding to the goethite from Rietra et al. (2001) given in Tables 2 and 3.

possible reason is that the interatomic distance information obtained through EXAFS can be insufficient as a definitive constraint on possible binding configurations (Catalano et al., 2006b).

In order to test how the results in Fig. 10a and b might depend on the specific goethite used, we carried out a second set of selenate model predictions for the two EXAFS experimental conditions using the surface chemical properties established above for the adsorption of selenate on a goethite from Rietra et al. (Fig. 9, Tables 2 and 3). These calculations are depicted in Fig. 10c and d. It can be seen in these figures that under acidic conditions only the inner-sphere species is dominant—a different result to those shown in Fig. 10a. The model predictions thus have a strong dependence on the type of goethite used. The calculations in Fig. 10a refer to Hayes's goethite under the EXAFS conditions examined by Hayes et al. (1987). It may well be that it is only for this (anomalous) goethite that an outer-sphere species is dominant at acid conditions at the ionic strength and surface coverage of the Hayes et al. EXAFS experiment. For the conditions of the Manceau and Charlet EXAFS experiments, both the Hayes and the Rietra goethites lead to the same conclusion, i.e. that an inner-sphere species is dominant. However, the exact nature of this species may not be predictable because it is not consistent with the type of inner-sphere species we have inferred for all the other goethites (and HFO) in the present study.

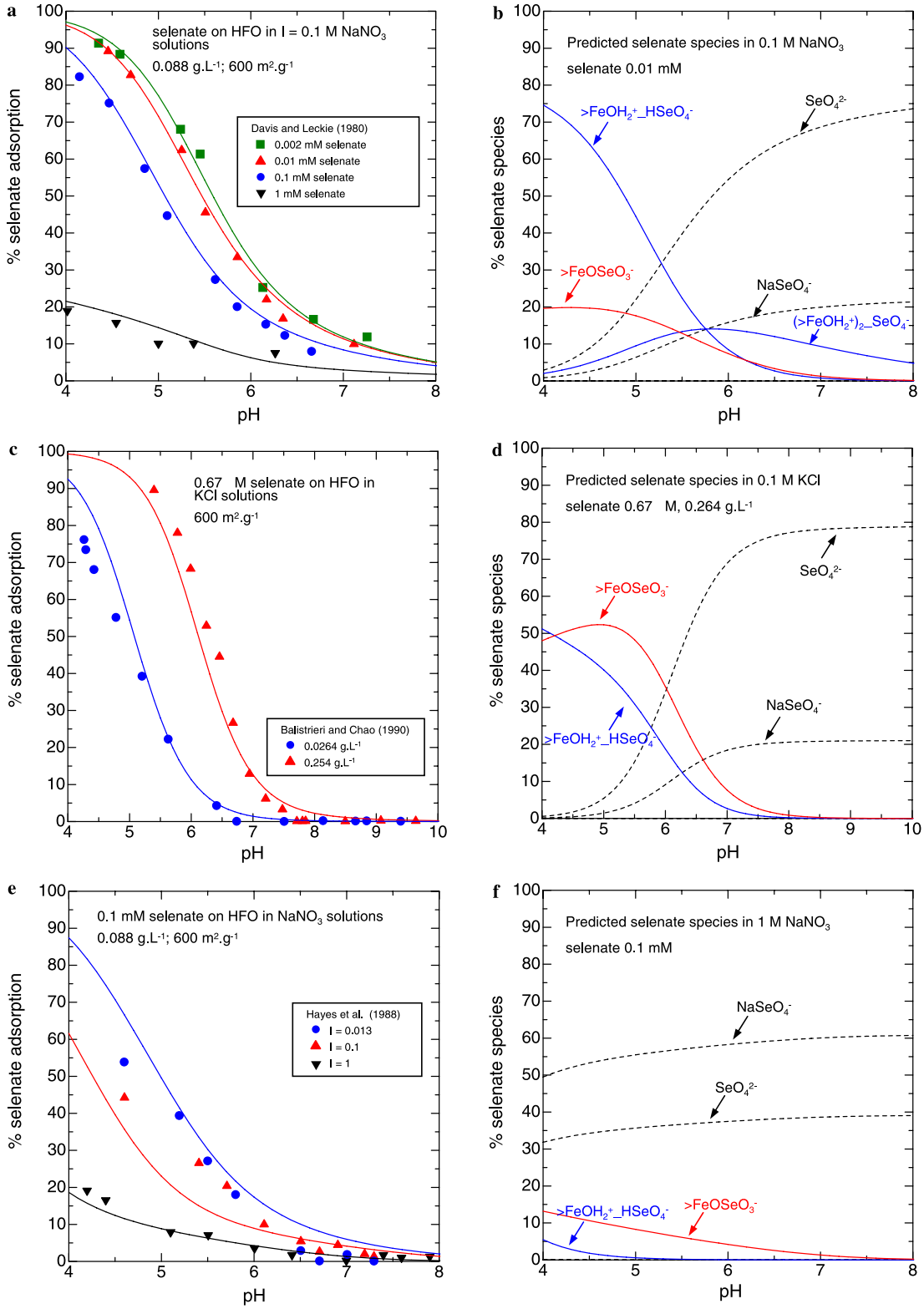

Fig. 11. The data points represent experimental results for selenate adsorption on HFO from Davis and Leckie (1980), Balistrieri and Chao (1990) and Hayes et al. (1988). The curves in (a, c, and d) represent regression calculations with the ETLM using the surface species and parameters in Tables 2 and 3. (a) Selenate adsorption as a function of pH and sulfate loading. (b) Predicted selenate speciation at 0.01 mM of selenate form (a). (c) Selenate adsorption as a function of pH and solid concentrations. (d) Predicted selenate speciation (0.0264 g L^{-1}) from (c). (e) Selenate adsorption as a function of pH and ionic strength. (f) Predicted selenate surface and aqueous speciation at $I = 1$ from (e).

3.3.4. Adsorption of selenate on HFO from Davis and Leckie (1980), Balistrieri and Chao (1990) and Hayes et al. (1988)

A wide range of surface coverages and ionic strengths for selenate adsorption on HFO is depicted by the data in Fig. 11a, c, and e. The solid lines in these figures represent regression calculations using the minimum number of selenate surface species from the group $>FeSeO_3^-$, $(>FeOH_2^+)_2$_SeO_4^{2-} and $>FeOH_2^+$_$HSeO_4^-$, all of which might be expected based on the studies of HFO and goethite described above. The data from Davis and Leckie (1980) were best fit using all three species because they cover such a wide range of conditions. However, the other two data sets only required two surface species. It can be seen in Fig. 11a, c, and e that the calculated curves provide close descriptions for the selenate adsorption envelopes on HFO over wide ranges of pH, surface coverage and ionic strength except for the data at $I = 0.1$ in Fig. 11e. The adsorption data for $I = 0.013$ and 0.1 in this figure show significant scatter, which may indicate substantial uncertainty in the data. Table 3 lists the parameters for selenate adsorption reactions on HFO. It is interesting to note that, as in the case of sulfate, the $\log K^{\theta}$ for HFO are higher than for goethite, indicating that HFO has a greater affinity for selenate than goethite.

The predicted model speciation of selenate on HFO are depicted in Fig. 11b, d, and f, respectively. The speciation plots refer to a range of surface coverages, ionic strengths and pH values. As in the case of selenate on goethite, the speciation plots in Fig. 11 indicate the dominant selenate surface species should depend very strongly on the environmental parameters.

4. Conclusions

The extended triple layer model (ETLM), which takes into account the electrostatics of water dipole desorption caused by inner-sphere surface complexation, was developed to help integrate published experimental spectroscopic and theoretical molecular evidence of the identity of oxyanion surface species with a surface complexation model of adsorption (Sverjensky and Fukushi, 2006a,b). With no additional fit parameters, the model is able to predict changes in the proportions of inner- and outer-sphere surface species with changes in environmental variables, such as pH, ionic strength and surface coverage, consistent with independent spectroscopic evidence. In the present study, the applicability of the ETLM to a wide variety of experimental adsorption, surface titration, and proton coadsorption data for sulfate and selenate on iron oxides under a wide range of conditions has been investigated. The goal was to determine the effect of pH, ionic strength, surface coverage and type of adsorbant on the surface speciation of sulfate and selenate on iron oxides consistent with evidence from FTIR and X-ray spectroscopic and theoretical molecular studies. In addition, the performance of the ETLM for integrating spectroscopic with bulk adsorption data is compared with the CD model. Based on the calculations described above, the following conclusions can be made.

(1) On seven out of eight goethites studied, sulfate and selenate surface reactions for a wide variety of different types of experimental data were successfully represented with the ETLM involving a monodentate-mononuclear inner-sphere and a bidentate-binuclear outer-sphere (or H-bonded) species according to

$$>FeOH + H^+ + AO_4^{2-} => FeOAO_3^- + H_2O$$

and

$$2>FeOH + 2H^+ + AO_4^{2-} = (>FeOH_2^+)_2\_AO_4^{2-} \qquad (23)$$

respectively, where A stands for S or Se. The model predicted changes in the proportions of the species with pH, ionic strength and surface coverage consistent with independently derived experimental evidence from *in situ* Raman, ATR-FTIR, and EXAFS studies. Only one goethite (Hayes et al., 1988) required a slightly different surface speciation involving a protonated outer-sphere (or H-bonded) selenate species.

(2) The reactions given above involving a monodentate-mononuclear inner-sphere and a bidentate-binuclear outer-sphere (or H-bonded) sulfate or selenate surface species are not only consistent with available spectroscopic evidence but also with the theoretical MO/DFT calculations of Paul et al. (2005). The latter had suggested also that a bidentate-binuclear sulfate species might be an alternative inner-sphere species. However, our calculations indicate that, within the constraints and limitations of the ETLM, such a species is not consistent with the bulk adsorption data. Consequently, taken together, the spectroscopic, MO/DFT and surface complexation evidence strongly support the reactions cited above involving the inner-sphere species $>FeOAO_3^-$ and the species $(>FeOH_2^+)_2$_AO_4^{2-}. In the present work, the latter species represents either an outer-sphere complex or a H-bonded species. Additional experimental and theoretical studies will be necessary to distinguish these possibilities.

(3) Although the wide variety of different types of goethites analysed in the present study involved the same types of surface selenate and sulfate species, the magnitudes of the derived equilibrium constants varied substantially, particularly for those goethites not synthesised under CO_2-free conditions. Site densities on goethite correlate with and can be predicted from surface area (see also Villalobos et al., 2003). The high BET (about $95\,m^2\,g^{-1}$), high pH_{ZPC} (9.3–9.4), CO_2-free goethites synthesized and characterized by Rietra and co-workers form an end-member in this series.

(4) For HFO, the ETLM analysis of sulfate and selenate adsorption required an additional outer-sphere (or H-bonded) surface species represented by,

$$>FeOH + 2H^+ + AO_4^{2-} => FeOH_2^+\_HAO_4^-$$

The regression values of $\log K^{\theta}$ (based on site-occupancy standard states) for $>FeOAO_3^-$ and $(>FeOH_2^+)_2\text{-}AO_4^{2-}$ on HFO are systematically higher than those on goethite, indicating that HFO has a greater affinity for sulfate and selenate than goethite.

(5) Comparison of the ETLM to CD model fits of sulfate and selenate adsorption on goethite indicated that under some circumstances the CD model can provide a closer fit to the experimental data, particularly when the CD model equilibrium constants and charge distribution parameters are obtained by regression. However, if the ETLM site density is known independently, the CD model requires double the number of fit parameters relative to the ETLM. Even under these circumstances the CD model is not sensitive to the number of surface species, not does it necessarily predict the correct changes in the proportions of surface species with changes in ionic strength (Rietra et al., 2001). In contrast, the ETLM is sensitive to the number of surface species because the electrostatic factor is not a regression parameter. In addition, as already noted, it can predict the correct changes in surface speciation with environmental changes.

(6) The predicted model speciation of selenate on goethite for the two different sets of conditions in the EXAFS studies of Hayes et al. (1987) and Manceau and Charlet (1994) helps to resolve the apparent differences of the two EXAFS studies. The lower ionic strength and higher surface coverage used by Hayes et al. (1987) is predicted to have favored an outer-sphere selenate species, whereas the higher ionic strength used by Manceau and Charlet (1994) is predicted to have favored an inner-sphere selenate species, as suggested by Peak and Sparks (2002). In addition, it appears that the (anomalous) surface properties of the goethite used by Hayes et al. may be a contributing factor.

Acknowledgments

We greatly appreciate discussions with Y. Arai, J.A. Davis, D.B. Kent, J. Kubicki , S. Myeneni, and G.A. Waychunas. We also value the detailed comments and suggestions made by three anonymous reviewers and the Associate Editor M. Machesky. Financial support was provided by DuPont Engineering and DOE Grant DE-FG02-96ER-14616.

Associate editor: Michael L. Machesky

References

Ali, M.A., Dzombak, D.A., 1996. Competitive sorption of simple organic acids and sulfate on goethite. *Environ. Sci. Technol.* **30** (4), 1061–1071.

Antelo, J., Avena, M., Fiol, S., Lopez, R., Arce, F., 2005. Effects of pH and ionic strength on the adsorption of phosphate and arsenate at the goethite–water interface. *J. Coll. Interf. Sci.* **285** (2), 476–486.

Arai, Y., Sparks, D.L., Davis, J.A., 2004. Effects of dissolved carbonate on arsenate adsorption and surface speciation at the hematite–water interface. *Environ. Sci. Technol.* **38** (3), 817–824.

Balistrieri, L.S., Chao, T.T., 1990. Adsorption of selenium by amorphous iron oxyhydroxide and manganese dioxide. *Geochim. Cosmochim. Acta* **54**, 739–751.

Balistrieri, L.S., Murray, J.W., 1981. The surface chemistry of goethite (α-FeOOH) in major ion seawater. *Am. J. Sci.* **281**, 788–806.

Bargar, J.R., Kubicki, J.D., Reitmeyer, R., Davis, J.A., 2005. ATR-FTIR spectroscopic characterization of coexisting carbonate surface complexes on hematite. *Geochim. Cosmochim. Acta* **69**, 1527–1542.

Blesa, M.A., Weisz, A.D., Morando, P.J., Salfity, J.A., Magaz, G.E., Regazzoni, A.e., 2000. The interaction of metal oxide surfaces with complexing agents dissolved in water. *Coord. Chem. Rev.* **196**, 31–63.

Breeuwsma, A., Lyklema, J., 1973. Physical and chemical adsorption of ions in the electrical double layer on hematite (α-Fe_2O_3). *J. Coll. Interf. Sci.* **43**, 437–448.

Catalano, J.G., Park, C., Zhang, Z., Fenter, P., 2006a. Termination and water adsorption at the α-Al_2O_3 (012)-aqueous solution interface. *Langmuir* **22**, 4668–4673.

Catalano, J.G., Zhang, Z., Fenter, P., Bedzyk, M.J., 2006b. Inner-sphere adsorption geometry of Se(IV) at the hematite (100)–water interface. *J. Coll. Interf. Sci.* **297**, 665–671.

Criscenti, L.J., Sverjensky, D.A., 1999. The role of electrolyte anions ClO_4^-, NO_3^-, and Cl^- in divalent metal (M2+) adsorption on oxide and hydroxide surfaces in salt solutions. *Am. J. Sci.* **299**, 828–899.

Criscenti, L.J., Sverjensky, D.A., 2002. A single-site model for divalent and heavy metal adsorption over a range of metal concentrations. *J. Coll. Interf. Sci.* **253**, 329–352.

Davis, J.A., Leckie, J.O., 1978a. Effect of adsorbed complexing ligands on trace metal uptake by hydrous oxides. *Environ. Sci. Technol.* **12**, 1309–1315.

Davis, J.A., Leckie, J.O., 1978b. Surface ionization and complexation at the oxide/water interface II. Surface properties of amorphous iron oxyhydroxide and adsorption of metal ions. *J. Coll. Interf. Sci.* **67**, 90–107.

Davis, J.A., Leckie, J.O., 1980. Surface ionization and complexation at the oxide/water interface 3. Adsorption of anions. *J. Coll. Interf. Sci.* **74**, 32–43.

Dzombak, D.A., Morel, F.M.M., 1990. *Surface Complexation Modeling*. John Wiley and Sons.

Elzinga, E.J., Peak, D., Sparks, D.L., 2001. Spectroscopic studies of Pb(II)–sulfate interactions at the goethite–water interface. *Geochim. Cosmochim. Acta* **65** (14), 2219–2230.

Fenter, P., Cheng, L., Rihs, S., Machesky, M., Bedyzk, M.D., Sturchio, N.C., 2000. Electrical double-layer structure at the rutile–water interface as observed in situ with small-period X-ray standing waves. *J. Coll. Interf. Sci.* **225**, 154–165.

Gaboriaud, F., Erhardt, J.-J., 2003. Effects of different crystal faces on the surface charge of colloidal goethite (a-FeoOOH) particles: an experimental and modeling study. *Geochim. Cosmochim. Acta* **67**, 967–983.

Geelhoed, J.S., Hiemstra, T., Riemsdijk, W.H.V., 1998. Competitive interaction between phosphate and citrate on goethite. *Environ. Sci. Technol.* **32**, 2119–2123.

Geelhoed, J.S., Hiemstra, T., van Riemsdijk, W.H., 1997. Phosphate and sulfate adsorption on goethite: single anion and competitive adsorption. *Geochim. Cosmochim. Acta* **61**, 2389–2396.

Goldberg, S., Johnston, C.T., 2001. Mechanisms of arsenic adsorption on amorphous oxides evaluated using macroscopic measurements, vibrational spectroscopy, and surface complexation modeling. *J. Coll. Interf. Sci.* **234**, 204–216.

Hansmann, D.D., Anderson, M.A., 1985. Using electrophoresis in modeling sulfate, selenite, and phosphate adsorption onto goethite. *Environ. Sci. Technol.* **19**, 544–551.

Hayes, K.F., 1987. Equilibrium, spectroscopic, and kinetic studies of ion adsorption at the oxide–aqueous interface. Ph.D., 260 pp., Stanford University.

Hayes, K.F., Papelis, C., Leckie, J.O., 1988. Modeling ionic strength effects on anion adsorption at hydrous oxide/solution interfaces. *J. Coll. Interf. Sci.* **125**, 717–726.

Hayes, K.F., Roe, A.L., Brown Jr., G.A., Hodgson, K.O., Leckie, J.O., Parks, G.A., 1987. In situ X-ray absorption study of surface complexes: selenium oxyanions on α-FeOOH. *Science* **238**, 783–786.

Helgeson, H.C., Kirkham, D.H., Flowers, G.C., 1981. Theoretical prediction of the thermodynamic behavior of aqueous electrolytes at high pressures and temperatures. IV. Calculation of activity coefficients, osmotic coefficients, and apparent molal and standard and relative partial molal properties to 5 kb and 600 °C. *Am. J. Sci.* **281**, 1241–1516.

Hiemstra, T., van Riemsdijk, W.H., 1996. A surface structural approach to ion adsorption: the charge distribution (CD) model. *J. Coll. Interf. Sci.* **179**, 488–508.

Hiemstra, T., van Riemsdijk, W.H., 1999. Surface structural ion adsorption modeling of competitive binding of oxyanions by metal (hydr)oxides. *J. Coll. Interf. Sci.* **210**, 182–193.

Hiemstra, T., van Riemsdijk, W.H., 2000. Fluoride adsorption on goethite in relation to different types of surface sites. *J. Coll. Interf. Sci.* **225**, 94–104.

Hug, S.J., 1997. In situ Fourier transform infrared measurements of sulfate adsorption on hematite in aqueous solutions. *J. Coll. Interf. Sci.* **188**, 415–422.

Liu, F., He, J.Z., Colombo, C., Violante, A., 1999. Competitive adsorption of sulfate and oxalate on goethite in the absence or presence of phosphate. *Soil Sci.* **164** (3), 180–189.

Majzlan, J., Myneni, S.C.B., 2005. Speciation of iron and sulfate in acid waters: aqueous clusters to mineral precipitates. *Environ. Sci. Technol.* **39** (1), 188–194.

Manceau, A., Charlet, L., 1994. The mechanism of selenate adsorption on goethite and hydrous ferrous oxide. *J. Coll. Interf. Sci.* **168**, 87–93.

Myneni, S.C.B., Tokunaga, T.K., Brown, G.E., 1997. Abiotic selenium redox transformations in the presence of Fe(II,III) oxides. *Science* **278** (5340), 1106–1109.

Ostergren, J.D., Brown, J.G.E., Parks, G.A., Persson, P., 2000. Inorganic ligand effects on Pb(II) sorption to goethite (a-FeOOH) II. Sulfate. *J. Coll. Interf. Sci.* **225**, 483–493.

Paul, K.W., Borda, M.J., Kubicki, J.D., Sparks, D.L., 2005. Effect of dehydration on sulfate coordination and speciation at the Fe–(Hydr)oxide–water interface: a molecular orbital/density functional theory and Fourier transform infrared spectroscopic investigation. *Langmuir* **21** (24), 11071–11078.

Peak, D., Ford, R.G., Sparks, D.L., 1999. An in situ ATR-FTIR investigation of sulfate bonding mechanisms on goethite. *J. Coll. Interf. Sci.* **218**, 289–299.

Peak, D., Sparks, D.L., 2002. Mechanisms of selenate adsorption on iron oxides and hydroxides. *Environ. Sci. Technol.* **36** (7), 1460–1466.

Rahnemaie, R., Hiemstra, T., van Riemsdijk, W.H., 2006. Inner- and outer-sphere complexation of ions at the goethite-solution interface. *J. Coll. Interf. Sci.* **297** (2), 379–388.

Rietra, R., Hiemstra, T., van Riemsdijk, W.H., 1999a. The relationship between molecular structure and ion adsorption on variable charge minerals. *Geochim. Cosmochim. Acta* **63** (19–20), 3009–3015.

Rietra, R.P.J.J., Hiemstra, T., van Riemsdijk, W.H., 1999. Sulfate adsorption on goethite. *J. Coll. Interf. Sci.* **218**, 511–521.

Rietra, R.P.J.J., Hiemstra, T., van Riemsdijk, W.H., 2000. Electrolyte anion affinity and its effect on oxyanion adsorption on goethite. *J. Coll. Interf. Sci.* **229**, 199–206.

Rietra, R.P.J.J., Hiemstra, T., van Riemsdijk, W.H., 2001. Comparison of selenate and sulfate adsorption on goethite. *J. Coll. Interf. Sci.* **240**, 384–390.

Sahai, N., Sverjensky, D.A., 1998. GEOSURF: a computer program for forward modeling of adsorption on mineral surfaces in aqueous solution. *Comput. Geosci.* **24**, 853–873.

Seby, F., Potin-Gautier, M., Giffaut, E., Borge, G., Donard, O.F.X., 2001. A critical review of thermodynamic data for selenium species at 25 °C. *Chem. Geol.* **171**, 173–194.

Shock, E.L., Sassani, D.C., Willis, M., Sverjensky, D.A., 1997. Inorganic species in geologic fluids: correlations among standard molal thermodynamic properties of aqueous cations, oxyanions, acid oxyanions, oxyacids and hydroxide complexes. *Geochim. Cosmochim. Acta* **61**, 907–950.

Sigg, L., Stumm, W., 1980. The interaction of anions and weak acids with the hydrous goethite (α-FeOOH) surface. *Coll. Surf.* **2**, 101–117.

Suarez, D.L., Goldberg, S., Su, C., Manning, B.A., 1997. Evaluation of oxyanion adsorption mechanisms on oxides using FTIR spectroscopy and electrophoretic mobility. Abstracts of Papers of the American Chemical Society 213, 59-GEOC.

Sverjensky, D.A., 2005. Prediction of surface charge on oxides in salt solutions: revisions for 1:1 (M^{+}_{L}-) electrolytes. *Geochim. Cosmochim. Acta* **69** (2), 225.

Sverjensky, D.A., Fukushi, K., 2006a. Anion adsorption on oxide surfaces: inclusion of the water dipole in modeling the electrostatics of ligand exchange. *Environ. Sci. Technol.* **40**, 263–271.

Sverjensky, D.A., Fukushi, K., 2006b. A predictive model (ETLM) for As(III) adsorption and surface speciation on oxides consistent with spectroscopic data. Geochim. Cosmochim. Acta, in press.

Sverjensky, D.A., Shock, E.L., Helgeson, H.C., 1997. Prediction of the thermodynamic properties of aqueous metal complexes to 1000 °C and 5.0 kb. *Geochim. Cosmochim. Acta* **61**, 1359–1412.

Swedlund, P.J., Webster, J.G., 2001. Cu and Zn ternary surface complex formation with SO_4 on ferrihydrite and schwertmannite. *Appl. Geochem.* **16** (5), 503–511.

Swedlund, P.J., Webster, J.G., Miskelly, G.M., 2003. The effect of SO_4 on the ferrihydrite adsorption of Co, Pb and Cd: ternary complexes and site heterogeneity. *Appl. Geochem.* **18** (11), 1671–1689.

Venema, P., Hiemstra, T., van Riemsdijk, W.H., 1996. Comparison of different site-binding models for cation sorption: description of pH dependency, salt dependency, and cation–proton exchange. *J. Coll. Interf. Sci.* **181**, 45–59.

Villalobos, M., Leckie, J.O., 2001. Surface complexation modeling and FTIR study of carbonate adsorption to goethite. *J. Coll. Interf. Sci.* **235**, 15–32.

Villalobos, M., Trotz, M.A., Leckie, J.O., 2003. Variability in goethite surface site density: evidence from proton and carbonate sorption. *J. Coll. Interf. Sci.* **268** (2), 273–287.

Wijnja, H., Schulthess, C.P., 2000. Vibrational spectroscopy study of selenate and sulfate adsorption mechanisms on Fe and Al (hydr)oxide surfaces. *J. Coll. Interf. Sci.* **229** (1), 286–297.

Wijnja, H., Schulthess, C.P., 2002. Effect of carbonate on the adsorption of selenate and sulfate on goethite. *Soil Sci. Soc. Am. J.* **66** (4), 1190–1197.

Yates, D.E., Healy, T.W., 1975. Mechanism of anion adsorption at the ferric and chromic oxide/water interfaces. *J. Coll. Interf. Sci.* **52**, 222–228.

Zhang, P.C., Sparks, D.L., 1990. Kinetics and mechanisms of selenate and selenite adsorption/desorption at the goethite/water interface. *Environ. Sci. Technol.* **24**, 1848–1856.

Zhang, P.C., Sparks, D.L., 1990. Kinetics and mechanisms of sulfate adsorption/desorption on goethite using pressure-jump relaxation. *Soil Sci. Soc. Am. J.* **54**, 1266–1273.

Zhang, Z., Fenter, P., Cheng, L., Sturchio, N.C., Bedyzk, M.D., Predota, M., Bandura, A.V., Kubicki, J.D., Lvov, S.N., Cummings, P.T., Chialvo, A.A., Ridley, M.K., Benezeth, P., Anovitz, L., Palmer, D.A., Machesky, M., Wesolowski, D.J., 2004. Ion adsorption at the rutile–water interface: linking molecular and macroscopic properties. *Langmuir* **20**, 4954–4969.